Journal of Sound and Vibration 329 (2010) 5116–5146

Contents lists available at ScienceDirect

Journal of Sound and Vibration

journal homepage: www.elsevier.com/locate/jsvi

Modelling of linear wave propagation in spatial fluid filled pipe systems consisting of elastic curved and straight elements

A. Søe-Knudsen*, S.V. Sorokin

Department of Mechanical and Manufacturing Engineering, Aalborg University, Pontoppidanstraede 101, Aalborg East, DK 9220, Denmark

ARTICLE INFO

Article history:
Received 13 January 2010
Received in revised form
8 May 2010
Accepted 16 June 2010
Handling Editor: H. Ouyang
Available online 10 July 2010

ABSTRACT

This paper is concerned with the theoretical analysis of time harmonic dynamics of compound elastic pipes with and without internal fluid loading. Compound pipes are assembled as a sequence of segments, each of which has a constant curvature. As a prerequisite for the wave propagation analysis, dispersion equations are solved, Green's matrices are formulated and Somigliana's identities are derived for an isolated curved segment. The governing equations of wave motion of a compound pipe are obtained as an ensemble of the boundary integral equations for individual segments and the continuity conditions at their interfaces. The proposed methodology is validated in several benchmark problems and then applied for analysis of the periodicity effects. The results obtained for piping systems with a variable number of identical curved segments are put into the context of the classical Floquet theory. Brief parametric studies suggest that the curved inserts can be employed as a tool for the passive control of wave propagation in fluid-filled pipes, and their stop band characteristics may be tailored to reach desirable attenuation levels in prescribed frequency ranges.

© 2010 Elsevier Ltd. All rights reserved.

1. Introduction

Spatial pipe structures are widely used in virtually all industrial and domestic applications, from gas- and oil-transporting pipelines to household heating and water supply systems. A by-product of the operational effect of pumps and valves on such structures is generation of vibro-acoustic energy, which may be transmitted in the pipeline over a long distance and emit undesirable noise, for example, from a distant radiator. Spatial piping systems are typically composed of straight and curved segments, and analysis of the vibro-acoustic properties of curved pipes is requested to predict behaviour of assembled compound structures. Wave propagation in straight pipes with and without fluid inside is a well established area of research, whereas linear dynamics of curved pipes has been considered in fewer publications. This paper is focused at modelling wave propagation phenomena in curved pipes individually and in their combinations with other curved and straight elements, including periodicity effects. It reports results of the work that has been split into the four subtasks:

- Derivation of the governing equations for linear time harmonic dynamics of planar curved fluid filled pipe segments in their in-plane and out-of-plane motion.
- Assessment of the roles of internal fluid loading parameters, when the fluid has a relatively slow flow rate and low internal pressure, followed by simplification of the governing equations.

* Corresponding author. Tel.: +45 9940 7328; fax: +45 9815 1675.
E-mail address: ask@me.aau.dk (A. Søe-Knudsen).

0022-460X/$ - see front matter © 2010 Elsevier Ltd. All rights reserved.
doi:10.1016/j.jsv.2010.06.015

Nomenclature

A_i	fluid-filled area
A_p	solid area of the pipe cross section
c_f	sound speed in fluid
c_s	speed of the plane dilatation wave in the material of a pipe
d_o	the outer diameter of a pipe (characteristic length scale)
E	Young's modulus
G	Shear modulus
h	wall thickness of a pipe
J	axial moment of inertia
J_p	polar moment of inertia
k	wavenumber
K	non-dimensional wavenumber
p_i	internal pipe pressure
q	external distributed force/moment
Q	non-dimensional external distributed force/moment
R	radius of curvature of a pipe
s	the coordinate along pipe centreline
S	the non-dimensional coordinate along pipe centreline
t	time
u	displacement along x-axis
U	non-dimensional displacement along x-axis
U_f	internal fluid flow speed
v	displacement along y-axis
V	non-dimensional displacement along y-axis
w	displacement along z-axis
W	non-dimensional displacement along z-axis
α	rotation around x-axis
A	rotation around x-axis as function of s/d_o
β	rotation around y-axis
B	rotation around y-axis as function of s/d_o
γ	rotation around z-axis
Γ	rotation around z-axis as function of s/d_o
ε	ratio between d_o and R
ε_z	strain along z-axis
η	material loss factor
ν	Poisson's ratio
ρ_f	mass density of the fluid
ρ_s	mass density of the material of a pipe
ω	circular frequency
Ω	non-dimensional frequency

Note: The definition of local pipe cross section coordinate systems and sign conventions for forces and moments, is giving in Appendix A.

- Derivation of Green's matrices and boundary integral equations for a curved pipe segments in their time harmonic in-plane and out-of-plane motion.
- Application of the Floquet theory for predicting location of frequency stop bands in an infinite periodic structure composed of alternating straight and curved pipe segments and analysis of the energy flux in a compound structure containing a moderate number of the same repeated substructures inside and outside the predicted stop and pass bands.

The first two items in the list above are seen by the authors as a necessary preliminary work, requested for the consistency of the paper. To the best of the authors' knowledge, the last two items have not yet been thoroughly studied in the literature and, therefore, these aspects present the novelty of this contribution.

The organisation of the paper into sections reflects the sequel of these tasks. Besides, the brief literature survey needed to put reported results into the existing framework is presented in Section 2.

2. The models and the tools

The purpose of the brief literature survey reported in this section is to put the model and the methodology we employ into the context of existing state of the art in the field.

2.1. Modelling of curved pipes with and without internal fluid loading

In what follows, we discuss modelling of pipes of the circular cross-section with their centre-line being of the circular shape. Then, depending on the wave length scale (which is controlled by the excitation frequency), a pipe may be modelled either as an elastic toroidal shell or as a slender curved beam. Alongside, the quiescent or flowing fluid inside a pipe may be modelled either as a continuum with effects of viscosity and compressibility taken into account or as a lumped added mass.

Obviously, a model of the elastic toroidal shell filled in with flowing viscous fluid is the most general one. To the best of our knowledge, no publications dealing with analysis of propagation of linear waves in this coupled solid–fluid wave guide are available. However, in most of practically meaningful situations, substantial simplifications in modelling the shell and the fluid can reliably be made, which reduce a pipe to a Bernoulli–Euler curved beam with a 'plug flow' of fluid inside. This model has been extensively employed in the literature, and its excellent exposition can be found in the classical text by Païdoussis [1]. In particular, this formulation has been used by Misra et al. [2,3]. We have chosen this model as a starting point for analysis and it is elaborated in Section 3. The governing equations for the in-plane wave motion in a curved beam

without internal fluid loading can also be found in Walsh and White [4], Kang et al. [5], and Lee et al. [6]. The discussion of these models in comparison with the model we have employed is presented in Section 4.

Asymptotic reduction of equations of motion of an elastic toroidal shell to those of a curved beam and the assessment of validity ranges of this model lies beyond the scope of the present paper. It should just be pointed out that such an assessment for a simpler case of a straight elastic pipe (a cylindrical shell with internal fluid loading) may be found, for instance, in Sorokin et al. [7]. It is realistic to expect that for a reasonably slender circular pipe the range of applicability of an elementary beam model should not be much different than for a straight pipe with the same cross-section.

2.2. The methodology of analysis of time harmonic dynamics of curved pipes

Governing differential equations of elastic wave propagation in and vibrations of curved pipes have a unique and exact solution in the form of linear combination of exponential functions. Several alternative methods employ this exact solution in different formats to consider free or forced vibrations of uniform or non-uniform curved and/or straight beams (pipes). The most prominent difference between these methods is the way to incorporate evanescent waves. Standard spectral element methods in various modifications – Doyle [8], Banerjee [9], Lee et al. [10], Lee [11] – is based on the derivation of the dynamic stiffness matrix, which is subsequently employed for analysis of dynamics of structures exactly in the same way as the conventional stiffness matrix is used for static analysis in the finite element method. In these references, the transfer matrix is set up with all exponential functions used, and its elementary transformation yields the requested dynamic stiffness matrix. This straightforward approach is perfect for numerical implementation in degenerate cases when no evanescent waves are supported by the wave guide (the axial wave in a straight rod or pipe). However, as soon as evanescent waves are supported on top of the travelling ones (flexural waves in a straight beam or a pipe), this approach leads to numerical instabilities in analysis of dynamics of slender beams. The instabilities are caused by computing of exponents of very large positive arguments, inherently involved in the derivation of the transfer matrix. This drawback in employing the transfer matrix for derivation of the dynamic stiffness matrix has been noticed, and several authors – see, for instance, Kang et al. [5] and Lee et al. [6] – have suggested a more elaborated technique to obtain the dynamic stiffness matrix, which is based on the proper account on reflection, transmission and propagation of waves of all types.

Naturally, approximate methods (Ritz method, Galerkin method, and, in particular, finite element method) are also widely used for analysis of free and forced vibrations of uniform and compound piping systems. The detailed survey of literature, where these methods have been employed lies beyond the scope of this paper. However, it should be pointed out that the classical finite element methodology for analysis of dynamics of curved beams was developed already in Davis et al. [12]. In several examples reported in Sections 4 and 5, we refer to the finite element analysis by commercially available software ANSYS11 for benchmarking and validating the codes, which implement exact solutions we have obtained by the boundary integral equations method.

2.3. Power flow analysis and calculations of eigenfrequencies of curved beams

Analysis of linear dynamics of curved beams can be performed in two formulations: in terms of travelling waves and related energy transfer in infinite and/or semi-infinite structures and in terms of standing waves in structures of the finite length. Of course, the issues of the energy transfer become relevant also for finite structures as soon as their forced vibrations are addressed with the material losses taken into account.

It would be a difficult but not particularly practical task to survey very many references, where eigenfrequencies and eigenmodes of vibrations of curved beams or pipes have been analysed. Perhaps, it could be just noticed that such an analysis has become fairly straightforward, if not trivial, with commercially available finite elements codes. On the other hand, power flow in compound curved beams has been studied in fewer references. The excellent study of power transmission (or power flow) in homogeneous curved beams performing the in-plane motion is presented in Walsh and White [4], whereas the energy flow in compound planar structures consisting of curved and straight segments is studied in the already mentioned references Kang et al. [5] and Lee et al. [6]. All these three references are concerned only with the in-plane wave motion of curved beams, but it is a fairly straightforward matter to replicate the results for the out-of-plane wave motion of curved beams, which is obviously similar to, but completely uncoupled from the in-plane motion.

Wave motion in a compound beam of finite length can be treated as a superposition of transmitted and reflected travelling waves, so that the methodology derived for semi-infinite structures can readily be applied for the standing waves analysis. This is exactly what has been done in Kang et al. [5] and Lee et al. [6]. A helpful literature survey on the issues discussed in this subsection can be found in the former reference, pp. 19–21.

2.4. Floquet theory and periodicity effects

As is well known, the frequency stop bands exist in an infinitely long wave guide with periodic elements, and the energy transmission is impossible if the excitation frequency falls into these stop bands. The classical Floquet theory Brillouin [13]and Mead [14] is conveniently used for calculation of Bloch parameters (or propagation constants), which are all

complex-valued in stop bands. In a straight elastic pipe, periodicity can be produced by equally spaced supports or inertial attachments, as described in the comprehensive review Mead [15]. One more type of periodicity, which can also be used in a straight pipe, is alternation of material properties of its continuous segments, see, for example Sorokin and Ershova [16,17]. In a compound pipe with curved segments, periodicity can be generated by alternation of their curvature. Naturally, the model of an infinitely long periodic structure is an idealized one, and predictions obtained by the use of this model may not be directly applicable for the practical purposes, in particular, to prevent transmission of the vibro-acoustic energy in pipes by employing a limited number of inclusions.

In recent publications Sorokin and Ershova [16,17] and Sorokin et al. [7], it has been shown that substantial attenuation effect may be achieved with a small number of periodicity cells inserted in a wave guide. This result is particularly relevant to studies of wave propagation in piping systems with curved elements, because these elements may be placed in a limited volume. In these references, the methodology of boundary integral equations has been applied to analyse the elastic wave propagation in compound thin-walled structures with continuous inclusions. The level of suppression of the wave propagation is controlled by a number of the 'periodicity cells' embedded in a wave guide. As is shown, there is an excellent agreement between the Floquet theory predictions and the results of the energy transmission analysis in the considered semi-infinite compound structures.

2.5. The boundary integral equations method

In the present paper, we employ the boundary integral equations method as a tool for analysis of free and forced vibrations of finite or infinite uniform and compound piping systems. This method has been used by one of the coauthors for analysis of linear time harmonic motion of various quasi-one-dimensional wave guides (homogeneous beams, sandwich beams, homogeneous cylindrical shells—each of which both with and without heavy fluid loading) in a number of publications. This method has several characteristic features, which are summarized as follows. The boundary integral equations method for one dimensional domains yields algebraic rather than integral governing equations, and, therefore, it gives the exact solution of any one-dimensional problem. It is equally applicable for solving problems in the time harmonic response of infinitely long uniform structures and of structures composed of continuous segments with different properties. This method is equally applicable to consider travelling waves in infinite/semi-infinite structures and standing waves in structures of finite dimensions. Inasmuch as Green's matrices are set up with the radiation and decay conditions being taken into account, the algorithm of solving problems in time-harmonic response by boundary integral equations method is inherently stable.

3. Equations of motion of curved fluid-filled pipes

3.1. Curved fluid filled pipes

In the low-frequency range, a curved pipe can be modelled within the conventional theory of rods, which accounts for axial deformation, torsion and flexural deformation within Bernoulli–Euler theory as described in Love [18] (see also Wittrick [19] and Sorokin [20]). This formulation can be modified for curved pipe as suggested by Misra et al. [3], to include forces exerted at the walls of a pipe, by the internal fluid. This modification results in following six equations of motion for a fluid filled pipe segment:

$$\frac{\partial R_u}{\partial s}+\frac{1}{R}R_w+P_u=\rho_s A_p\frac{\partial^2 u}{\partial t^2} \tag{1}$$

$$\frac{\partial R_v}{\partial s}+P_v=\rho_s A_p\frac{\partial^2 v}{\partial t^2} \tag{2}$$

$$\frac{\partial R_w}{\partial s}-\frac{1}{R}R_u+P_w=\rho_s A_p\frac{\partial^2 z}{\partial t^2} \tag{3}$$

$$R_v=\frac{\partial M_\alpha}{\partial s}+\frac{1}{R}M_w-\alpha R_w \tag{4}$$

$$R_u=-\frac{\partial M_\beta}{\partial s}+\beta R_w \tag{5}$$

$$\frac{\partial M_\gamma}{\partial s}-\frac{1}{R}M_\alpha+\beta R_v+\alpha R_u=\rho_s J_p\frac{\partial^2 \gamma}{\partial t^2} \tag{6}$$

Here, P_u, P_v and P_w are 'fluid–structure interaction' forces. The angles of rotation due to flexure are defined in accordance with Bernoulli–Euler theory as

$$\alpha=-\frac{\partial v}{\partial s},\quad \beta=\frac{\partial u}{\partial s}+\frac{w}{R} \tag{7}$$

And M_β, R_w, M_α and M_γ are defined in accordance with the same Bernoulli–Euler theory as

$$M_\beta = EJ\left(\frac{\partial^2 u}{\partial s^2}+\frac{1}{R}\frac{\partial w}{\partial s}\right),\quad R_w = EA_p\left(\frac{\partial w}{\partial s}+\frac{u}{R}\right) \tag{8}$$

$$M_\alpha = EJ\left(-\frac{\partial^2 v}{\partial s^2}+\frac{\gamma}{R}\right),\quad M_\gamma = EJ_p\left(\frac{\partial \gamma}{\partial s}+\frac{1}{R}\frac{\partial v}{\partial s}\right) \tag{9}$$

The model formulated in [1,13] accounts for so-called 'plug flow' of the in effect inviscid fluid inside a pipe and, therefore, only for the force transmission in normal direction to the inner surface of a pipe. In view of these assumptions, the fluid velocity field is introduced as

$$\mathbf{V}_f = \left\lfloor \frac{\partial u}{\partial t}, \frac{\partial v}{\partial t}, U_f \right\rfloor^{\mathrm{T}} \tag{10}$$

Standard algebra (see Païdoussis [1] for details) yields the following four governing equations for the curved fluid filled pipe:

$$\begin{aligned}\left(\rho_s A_p+\rho_f A_i\right)\frac{\partial^2 u}{\partial t^2} = &\underline{\underline{-EJ\left(\frac{\partial^4 u}{\partial s^4}+\frac{1}{R}\frac{\partial^3 w}{\partial s^3}\right)-EA_p\left(\frac{1}{R^2}u-\frac{1}{R}\frac{\partial w}{\partial s}\right)}}-A_i p_i\left(\frac{\partial^2 u}{\partial s^2}+\frac{1}{R}\frac{\partial w}{\partial s}\right)\\ &-\rho_f A_i U_f^2\left(\frac{\partial^2 u}{\partial s^2}+\frac{1}{R}\frac{\partial w}{\partial s}\right)-2\rho_f A_i U_f\left(\frac{\partial^2 u}{\partial t\,\partial s}+\frac{1}{R}\frac{\partial w}{\partial t}\right)\end{aligned} \tag{11}$$

$$\begin{aligned}\rho_s A_p\frac{\partial^2 w}{\partial t^2} = &\underline{\underline{EA_p\left(\frac{\partial^2 w}{\partial s^2}-\frac{1}{R}\frac{\partial u}{\partial s}\right)+EJ\left(\frac{1}{R^2}\frac{\partial^2 w}{\partial s^2}+\frac{1}{R}\frac{\partial^3 u}{\partial s^3}\right)}}+A_i p_i\left(\frac{1}{R^2}w+\frac{1}{R}\frac{\partial u}{\partial s}\right)\\ &-\rho_f A_i U_f\frac{1}{R}\frac{\partial u}{\partial t}+\rho_f A_i U_f^2\left(\frac{1}{R^2}w+\frac{1}{R}\frac{\partial u}{\partial s}\right)\end{aligned} \tag{12}$$

$$\begin{aligned}\left(\rho_s A_p+\rho_f A_i\right)\frac{\partial^2 v}{\partial t^2} = &\underline{\underline{-EJ\left(\frac{\partial^4 v}{\partial s^4}-\frac{1}{R}\frac{\partial^2 \gamma}{\partial s^2}\right)+GJ_p\left(\frac{1}{R^2}\frac{\partial^2 v}{\partial s^2}+\frac{1}{R}\frac{\partial^2 \gamma}{\partial s^2}\right)}}-A_i p_i\frac{\partial^2 v}{\partial s^2}\\ &-2\rho_f A_i U_f\frac{\partial^2 v}{\partial t\,\partial s}-\rho_f A_i U_f^2\frac{\partial^2 v}{\partial s^2}\end{aligned} \tag{13}$$

$$\rho_s J_p\frac{\partial^2 \gamma}{\partial t^2} = \underline{\underline{GJ_p\left(\frac{\partial^2 \gamma}{\partial s^2}+\frac{1}{R}\frac{\partial^2 v}{\partial s^2}\right)-EJ\left(\frac{1}{R^2}\gamma-\frac{1}{R}\frac{\partial^2 v}{\partial s^2}\right)}} \tag{14}$$

The pair of Eqs. (11)–(12) describes the linear in-plane (x–z-plane) flexural–longitudinal motion of the pipe. The pair of Eqs. (13)–(14) describes the linear out-of-plane (y–z-plane) flexural–torsion motion.

As compared with equations in [1,13], the static deformation of a pipe produced by the component of pressure and the centrifugal force $(-1/R)\left(\rho_f A_i U_f^2+A_i p_i\right)$ is ignored. It restricts our analysis to the situation, when a fluid-filled pipe is sufficiently stiff to withstand the abovementioned forcing without changing its shape. This assumption is totally realistic for the overwhelming majority of industrial and domestic pipelines.

3.2. Dispersion diagrams

To assess the influence of the internal fluid parameters e.g., density, flow speed and internal pressure, on the linear dynamics of a fluid filled pipe, dispersion diagrams are plotted for curved pipes with a uniform circular cross-section in three different cases. These non-dimensional diagrams in the low frequency range are shown in Figs. 1–3 for wavenumbers of in-plane and out-of-plane motion. In each case, one of the fluid parameters is varied while the other two are kept constant. All the illustrated cases are for pipes where the fluid cross section area, A_i, is 10 times larger than the solid, A_p, and the relation ε between pipe curvature radius, R, and A_p is 0.1, where ε is given as

$$\varepsilon = \frac{d_o}{R},\quad d_o = \sqrt{\frac{4A_p}{\pi}} \tag{15}$$

The non-dimensional ratios for fluid mass, pressure, flow speed, frequency and wavenumber are given below:

$$B_\rho = \frac{\rho_f}{\rho_s},\quad B_p = \frac{p_i}{E},\quad B_U = \frac{U_f}{c_f},\quad B_A = \frac{A_i}{A_p},\quad B_E = \frac{c_f^2\rho_f}{E},\quad \boldsymbol{\Omega} = \frac{\omega d_o}{c_s},\quad K = kd_o \tag{16}$$

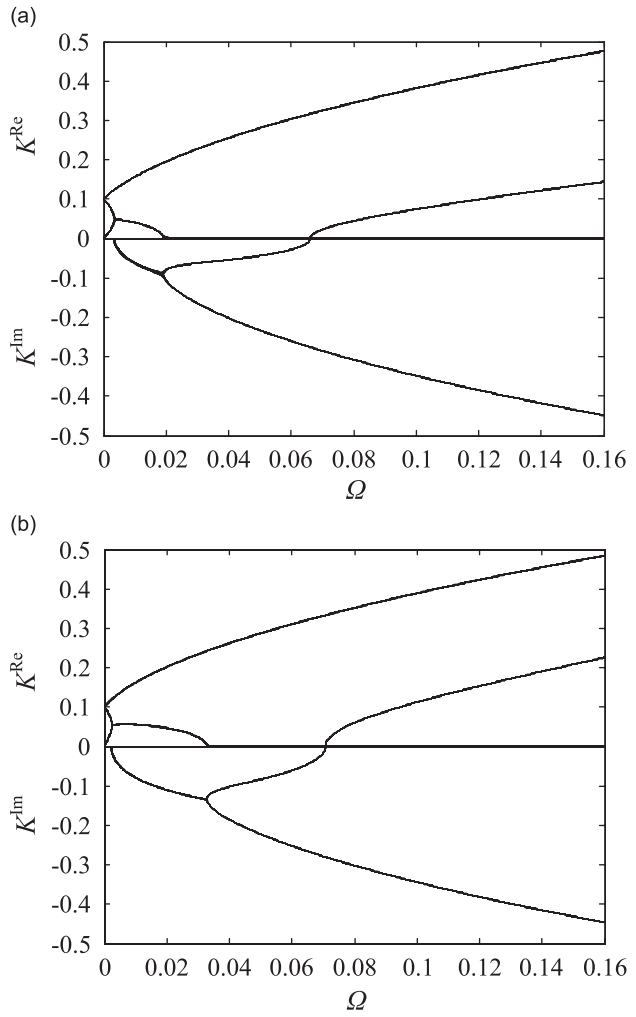

Fig. 1. Influence of the fluid speed on wavenumbers; flow speed ration B_U varied from 0 to (10/1400) in 10 steps, B_E=1000 · 1400^2/210e9, B_p=0 and B_ρ=1000/7800. Geometry parameters: B_A=10 and ε=0.1; (a) the in-plane case and (b) the out-of-plane case.

Solutions of linear differential equations Eqs. (11)–(14) is sought in the standard form:

$$\begin{aligned} u(s,t) &= \hat{U} d_o \exp(-i\omega t + iKS) \\ v(s,t) &= \hat{V} d_o \exp(-i\omega t + iKS) \\ w(s,t) &= \hat{W} d_o \exp(-i\omega t + iKS) \\ \gamma(s,t) &= \hat{\boldsymbol{\Gamma}} \exp(-i\omega t + iKS) \end{aligned} \tag{17}$$

where the scaled coordinate is defined as

$$S = \frac{s}{d_o} \tag{18}$$

The dispersion equation for in-plane motion is

$$C_6 K^6 + C_4 K^4 + C_3 K^3 + C_2 K^2 + C_1 K + C_0 = 0 \tag{19}$$

where C_j are given by

$$C_6 = \underline{\underline{1+2B_A}}$$

$$C_4 = \underline{\underline{-\Omega^2(1+2B_A) - 2\varepsilon^2(1+2B_A)}} - 16B_A(B_p + B_E B_U^2)$$

$$C_3 = \Omega B_A B_U \sqrt{B_\rho B_E}(32 - \varepsilon^2 - 2\varepsilon^2 B_A)$$

$$C_2 = \underline{\underline{\Omega^2 B_A(-2\varepsilon^2 - \varepsilon^2 B_\rho - 16B_\rho - 2\varepsilon^2 B_A B_\rho) - \Omega^2(\varepsilon^2 + 16) + \varepsilon^4(1+2B_A)}}$$

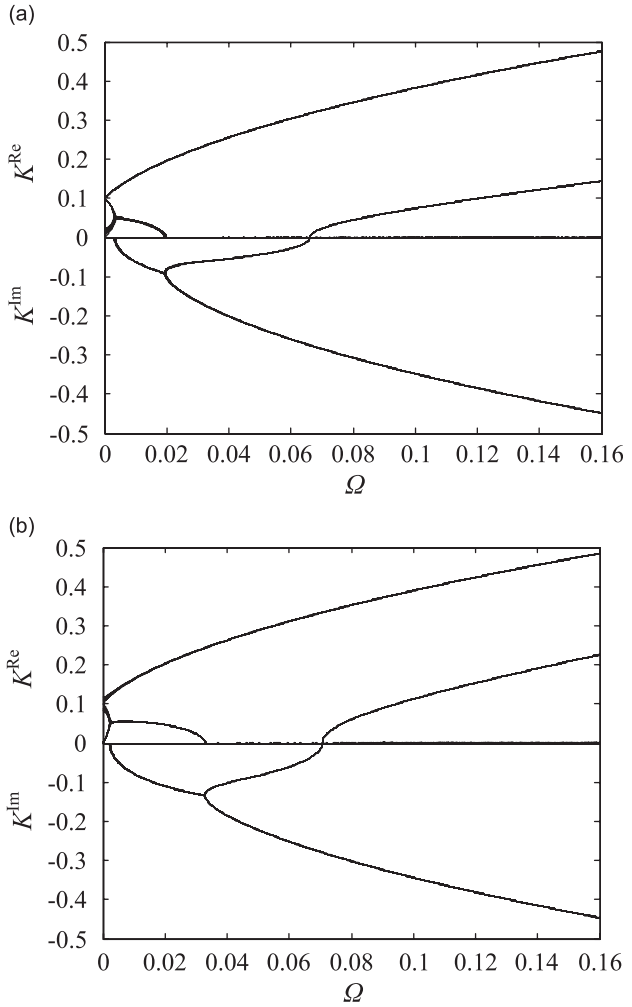

Fig. 2. Influence of internal pressure on wavenumbers; pressure ratio B_p varied from 0 to (160e5/210e9) in 10 steps, B_U=0 and B_ρ=1000/7800. Geometry parameters: B_A=10 and ε=0.1; (a) the in-plane case and (b) the out-of-plane case.

$$+\Omega^2 B_A(16B_p+16B_E B_U^2)+\varepsilon^2 32(B_p+B_A B_E B_U^2)$$
$$C_1=\Omega B_A B_U\sqrt{B_\rho B_E}(16\varepsilon^2 B_A B_p+16\varepsilon^2 B_A B_U^2 B_E-48\varepsilon^2-32\Omega^2)$$
$$C_0=\underline{\underline{-16\varepsilon^2\Omega^2+16\Omega^4(1+B_A B_\rho)}}$$
$$+16\varepsilon^2\Omega^2(B_A B_p-B_A^2 B_\rho B_E B_U^2+B_A^2 B_\rho B_p+B_A B_E B_U^2)-16\varepsilon^4 B_A(B_p+B_E B_U^2) \tag{20}$$

and for the out-of-plane motion it is

$$D_6K^6+D_4K^4+D_3K^3+D_2K^2+D_1K+D_0=0 \tag{21}$$

Here D_j are given by

$$D_6=\underline{\underline{1+2B_A}}$$
$$D_4=\underline{\underline{-\Omega^2(1+2B_A)2(1+\nu)-2\varepsilon^2(1+2B_A)}}-16B_A(B_p+B_E B_U^2)$$
$$D_3=32\Omega B_A B_U\sqrt{B_\rho B_E}$$
$$D_2=\underline{\underline{\Omega^2 B_A(-16B_\rho-4\varepsilon^2)-\Omega^2(2\varepsilon^2+16)+\varepsilon^4(1+2B_A)}}$$
$$+8B_A(B_U^2B_E+B_p)(2\Omega^2-\varepsilon^2)2(1+\nu)$$
$$D_1=32\Omega B_A B_U\sqrt{B_\rho B_E}(\varepsilon^2-2\Omega^2)(1+\nu)$$
$$D_0=\underline{\underline{16\Omega^2(1+\nu)(2\Omega^2-\varepsilon^2)(1+B_A B_\rho)}} \tag{22}$$

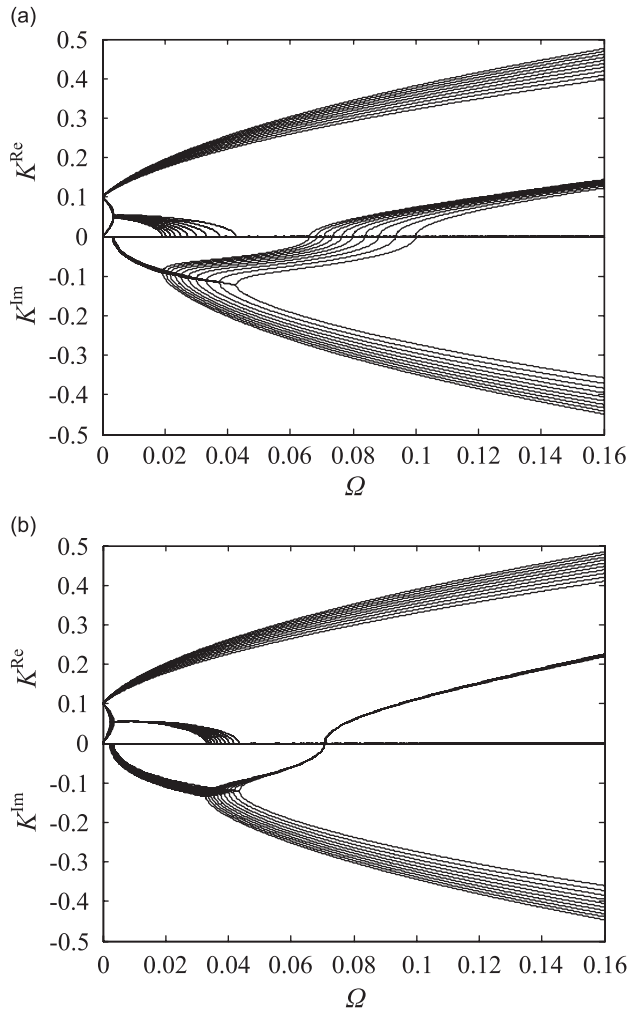

Fig. 3. Influence of the fluid mass density on wavenumbers; mass density ratio B_ρ varied from 0 to (1000/7800) in 10 steps, B_p=0 and B_U=0. Geometry parameters: B_A=10 and ε=0.1; (a) the in-plane case and (b) the out-of-plane case.

In each graph, the non-dimensional fluid parameter varies from zero up to a value corresponding to a water-filled steel pipe with the internal fluid flow speed of 10 m/s and internal static pressure of 160 bar in ten equally large steps. This is assumed to be within the operational limits for a typical fluid-filled pipe system. To give a relevance to pipes typically used in applications, we consider wave propagation in a pipe with the outer diameter of 60 mm, the wall thickness of 1.4 mm and the radius of curvature, R=0.18 m in the frequency range up to 7294 Hz.

It can be seen that changes in the mass ratio B_ρ generate a significantly larger change in location of the dispersion curves, than changes in the pressure ratio B_p and in the flow speed ratio B_U. It is therefore concluded that the influence of the fluid flow speed and the static fluid pressure may be ignored in the further analysis. This simplifies the governing equations, Eqs. (11)–(14), for the curved fluid filled pipe so that only underlined terms should be kept. The same is done for the two dispersion polynomials, Eq. (20) for the in-plane motion and Eq. (22) for the out-of-plane motion, in which only the underlined terms are taken into account.

3.3. Modal coefficients

In what follows, the non-dimensional forces, moments are defined as

$$\hat{R} = R\frac{1}{EA_p}, \quad \hat{M} = M\frac{1}{EA_p d_o} \tag{23}$$

The non-dimensional displacements and rotations are expressed via their dimensional counterparts as follows:

$$\begin{gathered} U(S) = \frac{u(s)}{d_o}, \quad V(S) = \frac{v(s)}{d_o}, \quad W(S) = \frac{w(s)}{d_o} \\ \mathrm{A}(S) = \alpha(s), \quad \mathrm{B}(S) = \beta(s), \quad \Gamma(S) = \gamma(s) \end{gathered} \tag{24}$$

With time dependence taken as, $\exp(-i\omega t)$ the underlined part of Eqs. (11)–(14) becomes
For the in-plane motion:

$$-(1+B_\rho B_A)\Omega^2 U = -\frac{1+2B_A}{16}\left(\frac{\partial^4 U}{\partial S^4}+\varepsilon\frac{\partial^3 W}{\partial S^3}\right)-\varepsilon^2 U+\varepsilon\frac{\partial W}{\partial S} \tag{25}$$

$$-\Omega^2 W = \frac{\partial^2 W}{\partial S^2}-\varepsilon\frac{\partial U}{\partial S}+\frac{1+2B_A}{16}\left(\varepsilon\frac{\partial^3 U}{\partial S^3}+\varepsilon^2\frac{\partial^2 W}{\partial S^2}\right) \tag{26}$$

For the out-of-plane motion:

$$-(1+B_\rho B_A)\Omega^2 V = -\frac{1+2B_A}{16}\left(\frac{\partial^4 V}{\partial S^4}-\varepsilon\frac{\partial^2 \Gamma}{\partial S^2}\right)+\frac{1+2B_A}{16(1+\nu)}\left(\varepsilon\frac{\partial^2 \Gamma}{\partial S^2}-\varepsilon^2\frac{\partial^2 V}{\partial S^2}\right) \tag{27}$$

$$-\frac{1+2B_A}{8}\Omega^2\Gamma = \frac{1+2B_A}{16(1+\nu)}\left(\frac{\partial^2 \Gamma}{\partial S^2}+\varepsilon\frac{\partial^2 V}{\partial S^2}\right)-\frac{1+2B_A}{16}\left(\varepsilon^2\Gamma-\varepsilon\frac{\partial^2 V}{\partial S^2}\right) \tag{28}$$

Dispersion equations (19) and (20) with only underlined terms retained can be derived from these two systems. For each root K_j^{ip} of the dispersion equation (19), the solution of equations (25) and (26) is

$$U_j(S)=\tilde{U}_j\exp(iK_j^{ip}S) \quad \text{and} \quad W_j(S)=\tilde{W}_j\exp(iK_j^{ip}S) \tag{29}$$

The amplitudes of the tangential and the normal displacements in this wave are linked by a modal coefficient, which has a simple explicit form:

$$\tilde{W}_j = im_j^w\tilde{U}_j$$
$$m_j^w = \frac{\varepsilon K_j^{ip}(16+(K_j^{ip})^2(1+2B_A))}{16(K_j^{ip})^2-16\Omega^2+\varepsilon^2(K_j^{ip})^2(1+2B_A)} \tag{30}$$

In the framework of the employed theory, the rotation angle associated with the in-plane bending is defined by the formula $\mathrm{B}=(\partial U/\partial S)+\varepsilon W$. Therefore, the modal coefficient of the in-plane rotation becomes

$$m_j^\beta = K_j^{ip}+\frac{\varepsilon^2 K_j^{ip}(16+(K_j^{ip})^2(1+2B_A))}{16(K_j^{ip})^2-16\Omega^2+\varepsilon^2(K_j^{ip})^2(1+2B_A)} \tag{31}$$

Thus, the kinematic variables in the free wave of in-plane deformation, which has a wavenumber K_j^{ip} are conveniently described by the vector of modal coefficients $\mathbf{m}_j^{ip}$:

$$\lfloor U_j, W_j, \mathrm{B}_j\rfloor^{\mathrm{T}} = \tilde{U}_j\mathbf{m}_j^{ip} \quad \text{where} \quad \mathbf{m}_j^{ip}=\left\lfloor 1,\ im_j^w \quad (iK_j^{ip}+i\varepsilon\, m_j^w)\right\rfloor^{\mathrm{T}} \tag{32}$$

The amplitude $\tilde{U}_j$ of this wave is determined by the excitation conditions.
The in-plane deformation of a circular pipe is characterized by two force resultants and a moment resultant, see (5), (8). Therefore, it is helpful to introduce the vector $\mathbf{n}_j^{ip}$ of modal coefficients of forces and moments associated with the free wave of the given wavenumber:

$$\left\lfloor \hat{R}_{uj}, \hat{R}_{wj}, \hat{M}_{\beta j}\right\rfloor^{\mathrm{T}} = \tilde{U}_j\mathbf{n}_j^{ip} \quad \text{where} \quad \mathbf{n}_j^{ip}=\left\{\begin{array}{l}\frac{1+2B_A}{16}\left(i(K_j^{ip})^3+i\varepsilon(K_j^{ip})^2 m_j^w\right)\\ -K_j^{ip}m_j^w-\varepsilon\\ \frac{1+2B_A}{16}\left(-(K_j^{ip})^2-\varepsilon K_j^{ip}m_j^w\right)\end{array}\right\} \tag{33}$$

Naturally, the forces and moments are proportional to the yet unknown amplitude $\tilde{U}_j$.

Exactly the same procedure is applied for the set of the out-of-plane waves. For each root K_j^{op} of the dispersion equation (21), the solution of equations (27)–(28) is

$$V_j(S)=\tilde{V}_j\exp(iK_j^{op}S) \quad \text{and} \quad \Gamma_j(S)=\tilde{\Gamma}_j\exp(iK_j^{op}S) \tag{34}$$

The amplitudes of the twist and the out-of-plane displacements in this wave are linked by a modal coefficient, which has a simple explicit form:

$$\tilde{\Gamma}_j = im_j^\gamma\tilde{V}_j$$
$$m_j^\gamma = \frac{i\varepsilon(K_j^{op})^2(2+\nu)}{K_j^2+(\varepsilon^2-2\Omega^2)(1+\nu)} \tag{35}$$

Taking into account that $A=-(\partial V/\partial S)$, the kinematic variables in the free wave of out-of-plane deformation, which has a wavenumber K_j^{op} are conveniently described by the vector of modal coefficients $\mathbf{m}_j^{op}$:

$$\left\lfloor V_j,\Gamma_j,A_j\right\rfloor^{\mathrm{T}}=\tilde{V}_j\mathbf{m}_j^{op}\quad\text{where}\quad\mathbf{m}_j^{op}=\left\lfloor 1,im_j^{\gamma},-iK_j^{op}\right\rfloor^{\mathrm{T}}\tag{36}$$

The amplitude $\tilde{V}_j$ of this wave is determined by the excitation conditions.

The out-of-plane deformation of a circular pipe is characterized by a force resultant and two moment resultants, see (4), (9). Therefore, it is helpful to introduce the vector $\mathbf{n}_j^{op}$ of modal coefficients of forces and moments associated with the free wave of the given wavenumber:

$$\left\lfloor\hat{R}_{\nu j},\hat{M}_{\gamma j},\hat{M}_{\alpha j}\right\rfloor^{\mathrm{T}}=\tilde{V}_j\mathbf{n}_j^{op}$$

$$\text{where}\quad\mathbf{n}_j^{op}=\left\{\begin{array}{l}\dfrac{1+2B_A}{16}\left(i(K_j^{op})^3-\varepsilon K_j^{op}m_j^{\gamma}\right)+\dfrac{1+2B_A}{16(1+\nu)}(-\varepsilon K_j^{op}m_j^{\gamma}+\varepsilon^2iK_j^{op})\\ \dfrac{1+2B_A}{16(1+\nu)}(-K_j^{op}m_j^{\gamma}+\varepsilon iK_j^{op})\\ \dfrac{1+2B_A}{16}\left((K_j^{\mathrm{op}})^2+i\varepsilon m_j^{\gamma}\right)\end{array}\right\}\tag{37}$$

By introducing the modal coefficients, we specify the sets of six in-plane waves and six out-of-plane waves. Their amplitudes are determined by the excitation and the boundary conditions.

3.4. Green's matrix

In what follows, non-dimensional distributed forces and distributed moments are defined as

$$Q_u=q_u\frac{d_o}{EA_p},\quad Q_\nu=q_\nu\frac{d_o}{EA_p},\quad Q_w=q_w\frac{d_o}{EA_p}$$
$$Q_\alpha=q_\alpha\frac{1}{EA_p},\quad Q_\beta=q_\beta\frac{1}{EA_p},\quad Q_\gamma=q_\gamma\frac{1}{EA_p}\tag{38}$$

When external distributed loading is taken into account, Eqs. (25)–(28) becomes

$$-(1+B_\rho B_A)\boldsymbol{\Omega}^2U=-\frac{1+2B_A}{16}\left(\frac{\partial^4U}{\partial S^4}+\varepsilon\frac{\partial^3W}{\partial S^3}\right)-\varepsilon^2U+\varepsilon\frac{\partial W}{\partial S}+Q_u-\frac{\partial Q_\beta}{\partial S}\tag{39}$$

$$-\boldsymbol{\Omega}^2W=\frac{\partial^2W}{\partial S^2}-\varepsilon\frac{\partial U}{\partial S}+\frac{1+2B_A}{16}\left(\varepsilon\frac{\partial^3U}{\partial S^3}+\varepsilon^2\frac{\partial^2W}{\partial S^2}\right)+Q_w+\varepsilon Q_\beta\tag{40}$$

$$-(1+B_\rho B_A)\Omega^2V=-\frac{1+2B_A}{16}\left(\frac{\partial^4V}{\partial S^4}-\varepsilon\frac{\partial^2\Gamma}{\partial S^2}\right)+\frac{1+2B_A}{16(1+\nu)}\left(\varepsilon\frac{\partial^2\Gamma}{\partial S^2}-\varepsilon^2\frac{\partial^2V}{\partial S^2}\right)+Q_\nu+\frac{\partial Q_\alpha}{\partial S}\tag{41}$$

$$-\frac{1+2B_A}{8}\Omega^2\Gamma=\frac{1+2B_A}{16(1+\nu)}\left(\frac{\partial^2\Gamma}{\partial S^2}+\varepsilon\frac{\partial^2V}{\partial S^2}\right)-\frac{1+2B_A}{16}\left(\varepsilon^2\Gamma-\varepsilon\frac{\partial^2V}{\partial S^2}\right)+Q_\gamma\tag{42}$$

The components of Green's matrix are defined as a response of an infinitely long structure to the excitation by a unit point force or a unit point moment modelled by Dirac's delta-function. The three in-plane loading cases and the three out-of-plane loading cases are listed in Table 1 and in Table 2, in this order.

In what follows, Green's matrices are derived for a homogenous infinitely long curved pipe. It means that its circular centerline is thought of as a helix with the pitch angle, which is equal to zero. In the case of the forced response, it implies that the waves travelling in the curved pipe from the excitation point in the opposite directions do not interact with each other as if they travel on different lists of Riemann surface. This concept allows simplification to the case of a straight pipe by letting the radius of a ring be infinitely large.

The set of loading cases is introduced with the Dirac delta-function $\delta(S-\xi)$, which is by definition dependent on the difference between two arguments, the coordinate of an observation point S, and the coordinate of the loading point ξ. It

Table 1
The three unit point load cases used for deriving the in-plane components in Green's matrix.

Along x axis	Along z axis	Around y axis
$Q_u=\delta(S-\xi)$	0	0
$Q_w=0$	$\delta(S-\xi)$	0
$Q_\beta=0$	0	$\delta(S-\xi)$

Table 2
The three unit point load cases used for deriving the out-of-plane components in Green's matrix.

Along y axis	Around z axis	Around x axis
$Q_v=\delta(S-\xi)$	0	0
$Q_\gamma=0$	$\delta(S-\xi)$	0
$Q_\alpha=0$	0	$\delta(S-\xi)$

has to be noticed that for a homogeneous pipe of constant curvature, the components of Green's matrices are also dependent on the distance between the observation and the excitation points, rather than upon each of them individually. More precisely, the arguments in the expressions for the components in Green's matrix are the following: the distance between observation and loading points $|S-\xi|$, and the location of the observation point with respect to excitation point, $\mathrm{sgn}(S-\xi)$. The latter dependence should be introduced for odd functions of the distance $|S-\xi|$.

As mentioned before, the equations of motion for the curved pipe are split into two independent sets, one for the in-plane case and another for the out-of plane case. The derivation of Green's matrix is split into the derivation of its two independent sub-matrices $\mathbf{G}^{ip}$ for the in-plane case and $\mathbf{G}^{op}$ for the out-of-plane case. Green's matrix is structured so that the components in the same row contain the same kinematic response for all unit point loading cases listed in Tables 1 and 2.

For example, the in-plane loading by a transverse unit force along the x-axis is defined by setting $Q_u=\delta(S-\xi)$, i.e. the internal transverse force $\hat{R}_u(S-\xi)$ experiences the jump from 1/2 when $S<\xi$ to $-1/2$ when $S>\xi$. Then the matrix element G^{ip}_{11} is the displacement $U(S-\xi)$ at S, G^{ip}_{21} is the displacement $W(S-\xi)$ and G^{ip}_{31} is the rotation $B(S-\xi)$. In the same way, the second column in $\mathbf{G}^{ip}$ is given for the $Q_w=\delta(S-\xi)$ load case and the third column is for the $Q_\beta=\delta(S-\xi)$ case. The components in $\mathbf{G}^{op}$ are defined similarly. Here $Q_v=\delta(S-\xi)$ defines the first column, $Q_\gamma=\delta(S-\xi)$ the second one and $Q_\alpha=\delta(S-\xi)$ the third. The first row here gives the displacement $V(S-\xi)$, the second row gives rotation $\Gamma(S-\xi)$ and the third row gives rotation $A(S-\xi)$:

$$\mathbf{G}^{ip}=\begin{bmatrix} G^{ip}_{11} & G^{ip}_{12} & G^{ip}_{13}\\ G^{ip}_{21} & G^{ip}_{22} & G^{ip}_{23}\\ G^{ip}_{31} & G^{ip}_{32} & G^{ip}_{33}\end{bmatrix} \tag{43}$$

$$\mathbf{G}^{op}=\begin{bmatrix} G^{op}_{11} & G^{op}_{12} & G^{op}_{13}\\ G^{op}_{21} & G^{op}_{22} & G^{op}_{23}\\ G^{op}_{31} & G^{op}_{32} & G^{op}_{33}\end{bmatrix} \tag{44}$$

Following the same methodology as for $\mathbf{G}^{ip}$ and $\mathbf{G}^{op}$ the matrices $\mathbf{F}^{ip}$ and $\mathbf{F}^{op}$ describing the reaction forces and moment at S are defined. F^{ip}_{11} gives the force $\hat{R}_u$ at the coordinate S, F^{ip}_{21} gives $\hat{R}_w$, etc.

$$\mathbf{F}^{ip}=\begin{bmatrix} F^{ip}_{11} & F^{ip}_{12} & F^{ip}_{13}\\ F^{ip}_{21} & F^{ip}_{22} & F^{ip}_{23}\\ F^{ip}_{31} & F^{ip}_{32} & F^{ip}_{33}\end{bmatrix} \tag{45}$$

$$\mathbf{F}^{op}=\begin{bmatrix} F^{op}_{11} & F^{op}_{12} & F^{op}_{13}\\ F^{op}_{21} & F^{op}_{22} & F^{op}_{23}\\ F^{op}_{31} & F^{op}_{32} & F^{op}_{33}\end{bmatrix} \tag{46}$$

The modal coefficients for the in-plane case are collected in matrix $\mathbf{M}^{ip}$, and these coefficients for the out of plane case are collected in $\mathbf{M}^{op}$;

$$\mathbf{M}^{ip}=\left[\mathbf{m}^{ip}_1,\mathbf{m}^{ip}_2,\mathbf{m}^{ip}_3\right],\quad \mathbf{M}^{op}=\left[\mathbf{m}^{op}_1,\mathbf{m}^{op}_2,\mathbf{m}^{op}_3\right] \tag{47}$$

The matrices $\mathbf{N}^{ip}$ and $\mathbf{N}^{op}$ are generated in the same way:

$$\mathbf{N}^{ip}=\left[\mathbf{n}^{ip}_1,\mathbf{n}^{ip}_2,\mathbf{n}^{ip}_3\right],\quad \mathbf{N}^{op}=\left[\mathbf{n}^{op}_1,\mathbf{n}^{op}_2,\mathbf{n}^{op}_3\right] \tag{48}$$

The nine components in each of the two Green's matrices $\mathbf{G}^{op}$ and $\mathbf{G}^{ip}$ can be presented in the general form:

$$G^{ip}_{kl}(S,\xi)\equiv G^{ip}_{kl}(S-\xi)=\sum_{j=1}^{3} M^{ip}_{kj}H^{ip}_{lj}\exp\left(iK^{ip}_j|S-\xi|\right)\chi^{ip}_{kl}$$

$$G^{op}_{kl}(S,\xi)\equiv G^{op}_{kl}(S-\xi)=\sum_{j=1}^{3} M^{op}_{kj}H^{op}_{lj}\exp\left(iK^{op}_j|S-\xi|\right)\chi^{op}_{kl}$$

where

$$k=1,2,3\quad\text{and}\quad l=1,2,3 \tag{49}$$

The components of the matrices $\boldsymbol{\chi}^{ip}$ and $\boldsymbol{\chi}^{op}$ are either 1 or sgn($S-\xi$). This choice defines whether the given component is an odd or an even function of $S-\xi$.

The matrices $\mathbf{F}^{ip}$ and $\mathbf{F}^{op}$ have similar form given as (49), where the components of the matrices $\boldsymbol{\varphi}^{ip}$ and $\boldsymbol{\varphi}^{op}$ are either 1 or sgn($S-\xi$). In the former case, the component of $\mathbf{F}^{ip}$ or $\mathbf{F}^{op}$ is an even function of $S-\xi$, in the latter case, it is an odd function:

$$F^{ip}_{kl}(S,\xi) \equiv F^{ip}_{kl}(S-\xi) = \sum_{j=1}^{3} N^{ip}_{kj} H^{ip}_{lj} \exp\left(iK^{ip}_{j}|S-\xi|\right)\varphi^{ip}_{kl}$$

$$F^{op}_{kl}(S,\xi) \equiv F^{op}_{kl}(S-\xi) = \sum_{j=1}^{3} N^{op}_{kj} H^{op}_{lj} \exp\left(iK^{op}_{j}|S-\xi|\right)\varphi^{op}_{kl}$$

where

$$k=1,2,3 \quad \text{and} \quad l=1,2,3 \tag{50}$$

In all the cases K_1, K_2 and K_3 are wavenumbers which satisfy the Sommerfeld radiation conditions and the decay conditions.

The selection of the three wavenumbers becomes clear by rewriting (17) so $K=(K^{\mathrm{Re}}+iK^{\mathrm{Im}})$ and $\xi=0$, $S=|S|$. It should also be observed that the dispersion polynomials for the in-plane and out-of-plane waves are of the sixth order each, and they contain only even powers of wavenumbers:

$$\begin{aligned}
u(s,t) &= \hat{U}d_o \exp(-K^{\mathrm{Im}}|S|)\left(\cos\left(K^{\mathrm{Re}}|S|-\omega t\right)+i\sin\left(K^{\mathrm{Re}}|S|-\omega t\right)\right)\\
v(s,t) &= \hat{V}d_o \exp\left(-K^{\mathrm{Im}}|S|\right)\left(\cos\left(K^{\mathrm{Re}}|S|-\omega t\right)+i\sin\left(K^{\mathrm{Re}}|S|-\omega t\right)\right)\\
w(s,t) &= \hat{W}d_o \exp\left(-K^{\mathrm{Im}}|S|\right)\left(\cos\left(K^{\mathrm{Re}}|S|-\omega t\right)+i\sin\left(K^{\mathrm{Re}}|S|-\omega t\right)\right)\\
\gamma(s,t) &= \hat{\Gamma} \exp\left(-K^{\mathrm{Im}}|S|\right)\left(\cos\left(K^{\mathrm{Re}}|S|-\omega t\right)+i\sin\left(K^{\mathrm{Re}}|S|-\omega t\right)\right)
\end{aligned} \tag{51}$$

If the imaginary part of a wavenumber does not vanish, $K^{\mathrm{Im}}\neq 0$, then the decay condition is satisfied for $K^{\mathrm{Im}}>0$. In the case, when the imaginary part of a wavenumber vanishes, $K^{\mathrm{Im}}=0$, the radiation condition should be employed. This condition is formulated with respect to the group velocity c_{group}, rather than to the phase velocity of wave propagation, and it states that the group velocity must be positive. A simple way to validate this condition is provided by the limit absorption principle, see Sveshnikov [21] and Vainberg [22]. If the material losses are introduced, Young's module becomes complex-valued (Rau [23]):

$$E_c = E(1-i\eta) \tag{52}$$

Then all wavenumbers become complex-valued, and the appropriate ones must obey the decay condition, i.e., $K^{\mathrm{Im}}>0$. As $\eta\to 0$, the imaginary parts of these wavenumbers also tend to zero, $K^{\mathrm{Im}}\to 0$ However, their real parts remain finite and the condition $c_{\mathrm{group}}>0$ holds true (see [21,22]). The expression for group velocity in this case is given here below:

$$\left.\begin{aligned}\hat{c}_{\mathrm{group}} = \frac{c_{\mathrm{group}}}{c_s} = \frac{\mathrm{d}\boldsymbol{\Omega}}{\mathrm{d}K}\\ K^{\mathrm{Im}}=0\end{aligned}\right\} \Rightarrow \hat{c}_{\mathrm{group}} = \frac{\mathrm{d}\boldsymbol{\Omega}}{\mathrm{d}K^{\mathrm{Re}}} \tag{53}$$

The components of matrices $\mathbf{H}^{ip}$, $\mathbf{H}^{op}$, $\boldsymbol{\chi}^{ip}$, $\boldsymbol{\chi}^{op}$, $\boldsymbol{\varphi}^{ip}$ and $\boldsymbol{\varphi}^{op}$ are determined as illustrated at Fig. 4 for the case where $Q_u(S)=\delta(S-\xi)$, $Q_w(S)=0$ and $Q_\beta(S)=0$.

The infinitely long curved pipe is divided to the two semi-infinite segments at the loading point ξ. Then a unit point force is evenly distributed between these segments and the appropriate continuity/symmetry conditions are formulated. It means that the internal force $\hat{R}_u(S-\xi)$ equals $-1/2$ at one side from the observation point, and the same force $\hat{R}_u(S-\xi)$ equals 1/2 at the other side to yield the required unit jump when the observation point comes across the loaded cross section of the pipe $S=\xi$ and, therefore, to balance the external unit load $Q_u(S)=\delta(S-\xi)$. This indicates that the internal

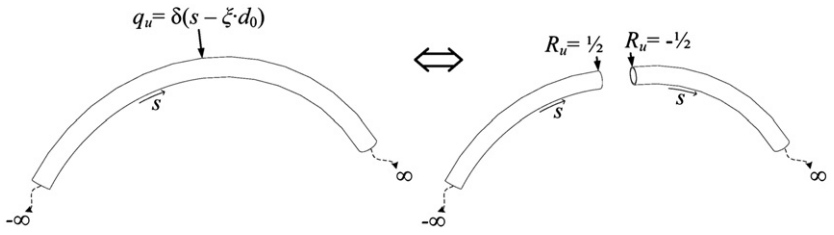

Fig. 4. The loading case $Q_u=\delta(S-\xi)$, $Q_w=0$, $Q_\beta=0$, $Q_v=0$, $Q_\gamma=0$ and $Q_\alpha=0$. The wavy arrows designate infinitely long segments.

force $\hat{R}_u(S-\xi)$ is the function, which is odd with respect to $S-\xi$ and discontinuous at $S=\xi$:

$$\hat{R}_u(S-\xi)=\frac{1+2B_A}{16}\left(-\frac{\partial^3 U}{\partial S^3}-\varepsilon\frac{\partial^2 W}{\partial S^2}\right)=-\frac{1}{2}\mathrm{sgn}(S-\xi)\quad\text{where}\quad S\to\xi \tag{54}$$

Therefore, it is necessary to choose $\varphi_{11}^{ip}=\mathrm{sgn}(S-\xi)$. The discontinuity condition (54) at the point $S=\xi$ specifies the loading case. Two additional conditions should be formulated at this point because it is necessary to determine the three coefficients H_{ij}^{ip} in Eqs. (49) and (50). These conditions are uniquely defined from the symmetry and continuity considerations.

To secure the continuity of all other components of Green's matrix belonging to the same load case, it is necessary to equate to zero at $S=\xi$ those, which are even functions. The components of Green's matrix are dependent on $|S-\xi|$, and, therefore, their differentiation with respect to S yields multiplication by $\mathrm{sgn}(S-\xi)$. Having this in mind, the odd and the even functions for a given loading case are easily indentified. As seen from Eq. (54), the force $\hat{R}_u(S-\xi)$ is an odd function. Then, obviously, the function $W(S-\xi)$ in this case must be odd, whereas the function $U(S-\xi)$ should be even. It suggests that $\chi_{11}^{ip}=1$ and $\chi_{21}^{ip}=\mathrm{sgn}(S-\xi)$. The rotation angle is defined by formula (7) right, and therefore, $\chi_{31}^{ip}=\mathrm{sgn}(S-\xi)$. Similar inspection into the structure of Eq. (8) suggests that are $\varphi_{21}^{ip}=1$ and $\varphi_{31}^{ip}=1$. A function, which is even in its argument $S-\xi$, is by definition continuous at $S=\xi$. A function, which is odd in its argument $S-\xi$, is continuous at $S=\xi$ if and only if it equals zero at this point. This is the way to uniquely specify the whole set of conditions at the loading point:

$$\begin{cases} F_{11}^{ip}\equiv\hat{R}_u(S-\xi)=-1/2\mathrm{sgn}(S-\xi) \\ G_{21}^{ip}\equiv W(S-\xi)=0 \\ G_{31}^{ip}\equiv \mathrm{B}(S-\xi)=0 \end{cases}\qquad\text{where}\quad S\to\xi \tag{55}$$

The remaining five sets of conditions for the unit point loading cases are presented in Appendix B. The expressions for $\mathbf{H}^{ip}$, $\mathbf{H}^{op}$, $\boldsymbol{\chi}^{ip}$, $\boldsymbol{\chi}^{op}$, $\boldsymbol{\varphi}^{ip}$ and $\boldsymbol{\varphi}^{op}$ are presented in Appendix C.

3.5. Reciprocity theorem and Somigliana's identities

The reciprocity theorem Wunderlich and Pilkey [24] is formulated here for the two loading cases of a curved pipe. The first one ('trial loading') is defined as a unit point loading case from Tables 1 and 2 for the unbounded pipe, and all state variables for this case are therefore available from Green's matrices as described in Section 3.4. The second loading case ('actual loading') is vibrations of a segment of the same pipe under given forces. The boundary conditions at its edges $S=a$ and $S=b$ are also given. If the prescribed forces are absent, the problem in forced response is reduced to the problem of free vibrations of the pipe of the given length with given boundary conditions at its edges.

For the in-plane case, the reciprocity theorem in the framework of Bernoulli–Euler theory is formulated as

$$\begin{aligned}&\int_a^b\left[\hat{R}_w\hat{\varepsilon}_w^o+\hat{M}_\beta\hat{\kappa}_\beta^o-\Omega^2WW^o-(1+B_\rho B_A)\Omega^2UU^o\right]\mathrm{d}S\\&=\int_a^b\left[\hat{R}_w^o\hat{\varepsilon}_w+\hat{M}_\beta^o\hat{\kappa}_\beta-\Omega^2W^oW-(1+B_\rho B_A)\Omega^2U^oU\right]\mathrm{d}S\end{aligned} \tag{56}$$

For the out-of-plane case it is

$$\begin{aligned}&\int_a^b\left[\hat{M}_\gamma\hat{\tau}_\gamma^o+\hat{M}_\alpha\hat{\kappa}_\alpha^o-\frac{1+2B_A}{8}\Omega^2\Gamma\Gamma^o-(1+B_\rho B_A)\Omega^2VV^o\right]\mathrm{d}S\\&=\int_a^b\left[\hat{M}_\gamma^o\hat{\tau}_\gamma+\hat{M}_\alpha^o\hat{\kappa}_\alpha-\frac{1+2B_A}{8}\Omega^2\Gamma^o\Gamma-(1+B_\rho B_A)\Omega^2V^oV\right]\mathrm{d}S\end{aligned} \tag{57}$$

After standard integration by parts and re-arranging the terms, reciprocity identity acquires the form of Eq. (58) for the in-plane case and the form of Eq. (59) for the out-of-plane case.

Here is the knowledge about the equations of motion, see Eqs. (39)–(42), taken into account. By doing so are the distributed loading terms introduced in the equations obtained by help of reciprocity as seen in the below two equations:

$$\begin{aligned}&\left|\hat{R}_wW^o+\hat{R}_uU^o+\hat{M}_\beta\mathrm{B}^o\right|_a^b+\int_a^b(Q_w+\varepsilon Q_\beta)W^o+\left(Q_u-\frac{\partial Q_\beta}{\partial S}\right)U^o\,\mathrm{d}S\\&=\left|\hat{R}_w^oW+\hat{R}_u^oU+\hat{M}_\beta^o\mathrm{B}\right|_a^b+\int_a^b(Q_w^o+\varepsilon Q_\beta^o)W+\left(Q_u^o-\frac{\partial Q_\beta^o}{\partial S}\right)U\,\mathrm{d}S\end{aligned} \tag{58}$$

where

$$\mathrm{B}=\frac{\partial U}{\partial S}+\varepsilon W$$
$$\hat{R}_w=\frac{\partial W}{\partial S}-\varepsilon U$$

$$\hat{R}_u = \frac{1+2B_A}{16}\left(-\frac{\partial^3 U}{\partial S^3} - \varepsilon\frac{\partial^2 W}{\partial S^2}\right)$$

$$\hat{M}_\beta = \frac{1+2B_A}{16}\left(\frac{\partial^2 U}{\partial S^2} + \varepsilon\frac{\partial W}{\partial S}\right)$$

$$Q_w + \varepsilon Q_\beta = -\frac{\partial^2 W}{\partial S^2} + \varepsilon\frac{\partial U}{\partial S} - \frac{1+2B_A}{16}\left(\varepsilon\frac{\partial^3 U}{\partial S^3} + \varepsilon^2\frac{\partial^2 W}{\partial S^2}\right) - \Omega^2 W$$

$$Q_u - \frac{\partial Q_\beta}{\partial S} = \frac{1+2B_A}{16}\left(\frac{\partial^4 U}{\partial S^4} + \varepsilon\frac{\partial^3 W}{\partial S^3}\right) - \varepsilon\frac{\partial W}{\partial S} + \varepsilon^2 U - (1+B_\rho B_A)\Omega^2 U$$

$$\begin{aligned}&\left|\hat{M}_\gamma \Gamma^o + \hat{R}_\nu V^o + \hat{M}_\alpha \mathrm{A}^o\right|_{\hat{a}}^{\hat{b}} + \int_a^b Q_\gamma \Gamma^o + \left(Q_\nu + \frac{\partial Q_\alpha}{\partial S}\right) V^o \,\mathrm{d}S \\ &= \left|\hat{M}_\gamma^o W + \hat{R}_\nu^o V + \hat{M}_\alpha^o \mathrm{A}\right|_a^b + \int_a^b Q_\gamma^o \Gamma + \left(Q_\nu^o + \frac{\partial Q_\alpha^o}{\partial S}\right) V \,\mathrm{d}S\end{aligned} \tag{59}$$

where

$$\mathrm{A} = -\frac{\partial V}{\partial S}$$

$$\hat{M}_\gamma = \frac{1+2B_A}{16(1+\nu)}\left(\frac{\partial \Gamma}{\partial S} + \varepsilon\frac{\partial V}{\partial S}\right)$$

$$\hat{R}_\nu = \frac{1+2B_A}{16}\left(-\frac{\partial^3 V}{\partial S^3} + \varepsilon\frac{\partial \Gamma}{\partial S}\right) + \frac{1+2B_A}{16(1+\nu)}\left(\varepsilon\frac{\partial \Gamma}{\partial S} + \varepsilon^2\frac{\partial V}{\partial S}\right)$$

$$\hat{M}_\alpha = \frac{1+2B_A}{16}\left(-\frac{\partial^2 V}{\partial S^2} + \varepsilon\Gamma\right)$$

$$Q_\gamma = -\frac{1+2B_A}{16(1+\nu)}\left(\frac{\partial^2 \Gamma}{\partial S^2} + \varepsilon\frac{\partial^2 V}{\partial S^2}\right) + \frac{1+2B_A}{16}\left(-\varepsilon\frac{\partial^2 V}{\partial S^2} + \varepsilon^2\Gamma\right) - \frac{1+2B_A}{8}\Omega^2\Gamma$$

$$Q_\nu + \frac{\partial Q_\alpha}{\partial S} = \frac{1+2B_A}{16}\left(\frac{\partial^4 V}{\partial S^4} - \varepsilon\frac{\partial^2 \Gamma}{\partial S^2}\right) - \frac{1+2B_A}{16(1+\nu)}\left(\varepsilon\frac{\partial^2 \Gamma}{\partial S^2} + \varepsilon^2\frac{\partial^2 V}{\partial S^2}\right) - (1+B_\rho B_A)\Omega^2 V$$

The boundary state variables (displacements, rotations, forces and moments at $S=a$ and $S=b$) for the 'trial loading' and for the 'actual loading' are contained in the reciprocity formulation, Eqs. (58) and (59). For the former case, they are explicitly formulated via components of Green's matrix (see Section 3.4). For the 'actual loading', displacements, rotations, forces and moments at the edges are either prescribed by the boundary conditions or should be found from the boundary integral equations.

The six Somigliana's identities for the curved pipe segment are presented in the matrix form as given below:

$$\mathbf{u}(\xi) = \mathbf{G}(a,\xi)\mathbf{r}_a + \mathbf{F}(a,\xi)\mathbf{u}(a) + \mathbf{G}(b,\xi)\mathbf{r}_b - \mathbf{F}(b,\xi)\mathbf{u}(b) + \mathbf{q}(\xi) \tag{60}$$

Here matrix $\mathbf{G}$ includes the components of $\mathbf{G}^{ip}$ and $\mathbf{G}^{op}$ and matrix $\mathbf{F}$ includes the components of $\mathbf{F}^{ip}$ and $\mathbf{F}^{op}$. The matrices $\mathbf{G}$, $\mathbf{F}$ and vectors $\mathbf{r}$, $\mathbf{u}$ and $\mathbf{q}$ are:

$$\mathbf{G}(S,\xi) = \begin{bmatrix} G_{11}^{ip}(S,\xi) & 0 & G_{21}^{ip}(S,\xi) & 0 & G_{31}^{ip}(S,\xi) & 0 \\ 0 & G_{11}^{op}(S,\xi) & 0 & G_{31}^{op}(S,\xi) & 0 & G_{21}^{op}(S,\xi) \\ G_{12}^{ip}(S,\xi) & 0 & G_{22}^{ip}(S,\xi) & 0 & G_{32}^{ip}(S,\xi) & 0 \\ 0 & G_{13}^{op}(S,\xi) & 0 & G_{33}^{op}(S,\hat{\xi}) & 0 & G_{23}^{op}(S,\xi) \\ G_{13}^{ip}(S,\xi) & 0 & G_{23}^{ip}(S,\xi) & 0 & G_{33}^{ip}(S,\xi) & 0 \\ 0 & G_{12}^{op}(S,\xi) & 0 & G_{32}^{op}(S,\xi) & 0 & G_{22}^{op}(S,\xi) \end{bmatrix} \tag{61}$$

$$\mathbf{F}(S,\xi) = \begin{bmatrix} F_{11}^{ip}(S,\xi) & 0 & F_{21}^{ip}(S,\xi) & 0 & F_{31}^{ip}(S,\xi) & 0 \\ 0 & F_{11}^{op}(S,\xi) & 0 & F_{31}^{op}(S,\xi) & 0 & F_{21}^{op}(S,\xi) \\ F_{12}^{ip}(S,\xi) & 0 & F_{22}^{ip}(S,\xi) & 0 & F_{32}^{ip}(S,\xi) & 0 \\ 0 & F_{13}^{op}(S,\xi) & 0 & F_{33}^{op}(S,\xi) & 0 & F_{23}^{op}(S,\xi) \\ F_{13}^{ip}(S,\xi) & 0 & F_{23}^{ip}(S,\xi) & 0 & F_{33}^{ip}(S,\xi) & 0 \\ 0 & F_{12}^{op}(S,\xi) & 0 & F_{32}^{op}(S,\xi) & 0 & F_{22}^{op}(S,\xi) \end{bmatrix} \tag{62}$$

$$\mathbf{u}(\xi) = \left\lfloor U(\xi), V(\xi), W(\xi), \mathrm{A}(\xi), \mathrm{B}(\xi), \Gamma(\xi)\right\rfloor^{\mathrm{T}} \tag{63}$$

$$\mathbf{r}_a = -\left\lfloor \hat{R}_u(a), \hat{R}_v(a), \hat{R}_w(a), \hat{M}_\alpha(a), \hat{M}_\beta(a), \hat{M}_\gamma(a) \right\rfloor^{\mathrm{T}} \tag{64}$$

$$\mathbf{r}_b = \left\lfloor \hat{R}_u(b), \hat{R}_v(b), \hat{R}_w(b), \hat{M}_\alpha(b), \hat{M}_\beta(b), \hat{M}_\gamma(b) \right\rfloor^{\mathrm{T}} \tag{65}$$

$$\mathbf{q}(\xi) = \begin{Bmatrix} \int_a^b \left(Q_u - \dfrac{\partial Q_\beta}{\partial S} \right) G_{11}^{ip}(S,\xi) + (Q_w + \varepsilon Q_\beta) G_{21}^{ip}(S,\xi)\, \mathrm{d}S \\ \int_a^b \left(Q_v + \dfrac{\partial Q_\alpha}{\partial S} \right) G_{11}^{op}(S,\xi) + Q_\gamma G_{21}^{op}(S,\xi)\, \mathrm{d}S \\ \int_a^b \left(Q_u - \dfrac{\partial Q_\beta}{\partial S} \right) G_{12}^{ip}(S,\xi) + (Q_w + \varepsilon Q_\beta) G_{22}^{ip}(S,\xi)\, \mathrm{d}S \\ \int_a^b \left(Q_v + \dfrac{\partial Q_\alpha}{\partial S} \right) G_{13}^{op}(S,\xi) + Q_\gamma G_{23}^{op}(S,\xi)\, \mathrm{d}S \\ \int_a^b \left(Q_u - \dfrac{\partial Q_\beta}{\partial S} \right) G_{13}^{ip}(S,\xi) + (Q_w + \varepsilon Q_\beta) G_{23}^{ip}(S,\xi)\, \mathrm{d}S \\ \int_a^b \left(Q_v + \dfrac{\partial Q_\alpha}{\partial S} \right) G_{12}^{op}(S,\xi) + Q_\gamma G_{22}^{op}(S,\xi)\, \mathrm{d}S \end{Bmatrix} \tag{66}$$

These identities are firstly used to derive boundary integral equations as explained in Section 3.6. As soon as all boundary state variables for the 'actual loading' case are found, these identities are re-used to calculate the displacements and rotations inside the given segment of a curved pipe. Differentiation of these identities with respect to the coordinate of the observation point ξ, and arrangement of derivatives in the form Eq. (62) yields the force and moment resultants inside the segment of a pipe. It should be emphasized that this differentiation is performed in the explicitly formulated components of Green's matrix. Therefore, the forces and the moment are determined exactly.

3.6. Boundary integral equations

The boundary integral equations for the state variables at the boundaries $S=a$ and $S=b$ of a given uniform segment of the compound pipe are obtained from Somigliana's identities (60) by letting the observation point, ξ tend to the boundaries $\xi=a+\mu$ and $\xi=b-\mu$, where $\mu\to 0$ and $a<b$. Thus, a system of twelve linear algebraic equations with respect to displacements, rotations, forces and moments at $S=a$ and $S=b$ is obtained. In the matrix form, vectors of boundary kinematic variables in the 'actual' state $\mathbf{u}(a)$ and $\mathbf{u}(b)$ are linked with the boundary forces and moments $\mathbf{r}_a$ and $\mathbf{r}_b$in this state as

$$\begin{Bmatrix} \mathbf{u}(a) \\ \mathbf{u}(b) \end{Bmatrix} = \begin{bmatrix} \mathbf{G}(a,a) & \mathbf{F}(a,\xi)\big|_{\xi=a+\mu} & \mathbf{G}(b,a) & -\mathbf{F}(b,a) \\ \mathbf{G}(a,b) & \mathbf{F}(a,b) & \mathbf{G}(b,b) & -\mathbf{F}(b,\xi)\big|_{\xi=b-\mu} \end{bmatrix} \begin{Bmatrix} \mathbf{r}_a \\ \mathbf{u}(a) \\ \mathbf{r}_b \\ \mathbf{u}(b) \end{Bmatrix} + \begin{Bmatrix} \mathbf{q}(a) \\ \mathbf{q}(b) \end{Bmatrix} \tag{67}$$

It is convenient to introduce the matrix:

$$\mathbf{B}_s \equiv \begin{bmatrix} \mathbf{G}(a,a) & (\mathbf{F}(a,\xi)\big|_{\xi=a+\mu} - \mathbf{I}) & \mathbf{G}(b,a) & -\mathbf{F}(b,a) \\ \mathbf{G}(a,b) & \mathbf{F}(a,b) & \mathbf{G}(b,b) & (-\mathbf{F}(b,\xi)\big|_{\xi=b-\mu} - \mathbf{I}) \end{bmatrix} \tag{68}$$

Then the boundary integral equations are re-formulated as follows:

$$\begin{Bmatrix} -\mathbf{q}(a) \\ -\mathbf{q}(b) \end{Bmatrix} = \mathbf{B}_s \begin{Bmatrix} \mathbf{r}_a \\ \mathbf{u}(a) \\ \mathbf{r}_b \\ \mathbf{u}(b) \end{Bmatrix} \tag{69}$$

In the case, when, for example $b\to\infty$, boundary state variables at $S=b$ are not introduced, and Eq. (69) becomes

$$-\mathbf{q}(a) = \begin{bmatrix} \mathbf{G}(a,a) & \mathbf{F}(a,\xi)\big|_{\xi=a+\mu} - \mathbf{I} \end{bmatrix} \begin{Bmatrix} \mathbf{r}_a \\ \mathbf{u}(a) \end{Bmatrix} \quad \text{where} \quad \mu\to 0 \tag{70}$$

Respectively, for the case, when $a\to\infty$, Eq. (69) becomes

$$-\mathbf{q}(b) = \begin{bmatrix} \mathbf{G}(b,b) & -\mathbf{F}(b,\xi)\big|_{\xi=b-\mu} - \mathbf{I} \end{bmatrix} \begin{Bmatrix} \mathbf{r}_b \\ \mathbf{u}(b) \end{Bmatrix} \quad \text{where} \quad \mu\to 0 \tag{71}$$

It should be noted that all components of the matrix $\mathbf{G}(S,\xi)\equiv\mathbf{G}(S-\xi)$ are continuous functions of the arguments, because they represent the displacements and rotations produced by a point force or a point moment. Off-diagonal components of

the matrix $\mathbf{F}(S,\xi)\equiv\mathbf{F}(S-\xi)$, which represents forces and moments generated in a structure in the trial loading case, are also continuous. However, the diagonal components of the matrix $\mathbf{F}(S,\xi)\equiv\mathbf{F}(S-\xi)$ are discontinuous functions at $S=\xi$, because they have to capture the unit jump in the force or in the moment at this loaded point. This discontinuity is taken into account by keeping the parameter μ in the boundary equations.

3.7. Interfacial continuity conditions and boundary conditions

The curved pipe segments may be either connected to each other in a sequential manner or connected to an 'outer' part of assembled piping system. In the former case, the set of interfacial continuity conditions should be formulated for all boundary state variables (displacements, rotations, forces and moments) at the interface between neighbouring segments.

Due to the chosen sign convention for the used boundary state variables, see Eq. (72), there are the following interfacial continuity conditions applied for all N sets of boundary states variables at the interfacial point, $\mathbf{r}_j$ containing boundary forces, moments and $\mathbf{u}_j$ containing boundary displacements, rotations:

$$\sum_{j=1}^{N}\mathbf{r}_j=0 \quad \text{and} \quad \mathbf{u}_j-\mathbf{u}_{j+1}=0 \tag{72}$$

The number of interfacial conditions is hereafter easily found as $6+6\cdot(N-1)$.

For the end segment of a pipe connected, say, to a radiator or a boiler, the set of conventional boundary conditions should be formulated. As seen in Eqs. (58) and (59), the boundary conditions for the in-plane deformation are formulated for the linear combinations of the following pairs $\hat{R}_w$ and W; $\hat{R}_u$ and U; $\hat{M}_\beta$ and B. For the out-on-plane deformation, the pairs are $\hat{M}_\gamma$ and Γ; $\hat{R}_v$ and V; $\hat{M}_\alpha$ and A.

3.8. The global system of linear algebraic equations for a compound curved pipe

Eqs. (69)–(71) are assembled with the given boundary and interfacial conditions into the following global system of linear algebraic equations describing the dynamics of a compound pipe system:

$$\mathbf{Bc}=\mathbf{q} \tag{73}$$

Solution of this system for $\mathbf{c}$ yields all boundary states variables in the 'actual loading' case for each segment. The displacements in each segment are then calculated straightforwardly by means of exact Somigliana's identities as described in the previous subsection.

The matrix–vector formulation presented in Eq. (69) can readily be transformed into the standard dynamical stiffness matrix form:

$$\mathbf{Z}^{-1}\begin{Bmatrix}\mathbf{q}(a)\\ \mathbf{q}(b)\end{Bmatrix}+\begin{Bmatrix}\mathbf{r}_a\\ \mathbf{r}_b\end{Bmatrix}=(-\mathbf{Z}^{-1}\mathbf{Y})\begin{Bmatrix}\mathbf{u}(a)\\ \mathbf{u}(b)\end{Bmatrix}$$

where

$$\mathbf{Z}=\begin{bmatrix}\mathbf{G}(a,a) & \mathbf{G}(b,a)\\ \mathbf{G}(a,b) & \mathbf{G}(b,b)\end{bmatrix}\mathbf{Y}=\begin{bmatrix}(\mathbf{F}(a,\xi)\big|_{\xi=a+\mu}-\mathbf{I}) & -\mathbf{F}(b,a)\big|\\ \mathbf{F}(a,b) & (-\mathbf{F}(b,\xi)\big|_{\xi=b-\mu}-\mathbf{I})\end{bmatrix} \tag{74}$$

for $\mu\to 0$

The matrix $(-\mathbf{Z}^{-1}\mathbf{Y})$ in Eq. (67) is the standard dynamical stiffness matrix. It is derived with the use of Green's matrix which satisfies the radiation and the decay conditions. This formulation of the dynamical stiffness matrix does not contain exponentially growing elements. It guarantees the numerical stability of computations.

3.9. Floquet theory formulation

An infinitely long periodic compound structure consisting of two or more alternating identical elements is considered. The equations of its free time-harmonic motion have the form of an infinitely large system of assembled boundary integral equations, which can be recognised as a periodic system of linear equations. The periodically repeated part of this equation system is the following sub-matrix system, where $n\in Z$:

$$0=\begin{bmatrix}\mathbf{J} & \mathbf{I} & & & 0\\ & \mathbf{B}_a & \mathbf{B}_c & \mathbf{B}_b & \\ 0 & & & \mathbf{J} & \mathbf{I}\end{bmatrix}\begin{Bmatrix}\mathbf{b}_{n-1}\\ \mathbf{a}_n\\ \mathbf{c}_n\\ \mathbf{b}_n\\ \mathbf{a}_{n+1}\end{Bmatrix} \quad \text{where} \quad \mathbf{J}=\begin{bmatrix}\mathbf{I} & 0\\ 0 & -\mathbf{I}\end{bmatrix} \tag{75}$$

Here $\mathbf{a}_n$ and $\mathbf{b}_n$ are vectors containing boundary state variables on each side of the 'n periodicity cell' and $\mathbf{c}_n$ contains its inner boundary state variables. Matrix $[\mathbf{B}_a, \mathbf{B}_c, \mathbf{B}_b]$ describes the assembled boundary integral equation matrix for such a single 'periodic cell'. As is known, a solution of a periodic linear system may be formulated as follows ([13–15,25]):

$$\mathbf{x}_n = \mathbf{x}_{n-m}\exp(miK_B) \quad \text{where} \quad \mathbf{x}_n = \left\lfloor \mathbf{b}_{n-1}^{\mathrm{T}}, \mathbf{a}_n^{\mathrm{T}}, \mathbf{c}_n^{\mathrm{T}}, \mathbf{b}_n^{\mathrm{T}}, \mathbf{a}_{n+1}^{\mathrm{T}} \right\rfloor^{\mathrm{T}} \tag{76}$$

In this formula, K_B is a propagation constant (Bloch parameter). The following equations may be written for three consecutive segments:

$$\lambda^1 \begin{Bmatrix} \mathbf{b}_{n-2} \\ \mathbf{a}_{n-1} \\ \mathbf{c}_{n-1} \\ \mathbf{b}_{n-1} \\ \mathbf{a}_n \end{Bmatrix} = \lambda^0 \begin{Bmatrix} \mathbf{b}_{n-1} \\ \mathbf{a}_n \\ \mathbf{c}_n \\ \mathbf{b}_n \\ \mathbf{a}_{n+1} \end{Bmatrix} = \lambda^{-1} \begin{Bmatrix} \mathbf{b}_n \\ \mathbf{a}_{n+1} \\ \mathbf{c}_{n+1} \\ \mathbf{b}_{n+1} \\ \mathbf{a}_{n+2} \end{Bmatrix} \quad \text{where} \quad \lambda^m = \exp(miK_B), \quad m \in Z \tag{77}$$

Then it is possible to reformulate Eq. (75) as follows:

$$0 = \begin{bmatrix} \mathbf{J} & \mathbf{I} & & & 0 \\ & \mathbf{B}_a & \mathbf{B}_c & \mathbf{B}_b & \\ 0 & & & \mathbf{J} & \mathbf{I} \end{bmatrix} \begin{Bmatrix} \lambda^{-1}\mathbf{b}_n \\ \mathbf{a}_n \\ \mathbf{c}_n \\ \mathbf{b}_n \\ \lambda\mathbf{a}_n \end{Bmatrix} \Leftrightarrow 0 = \begin{bmatrix} \mathbf{B}_a & \mathbf{B}_c & \mathbf{B}_b \\ \lambda\mathbf{I} & 0 & \mathbf{J} \end{bmatrix} \begin{Bmatrix} \mathbf{a}_n \\ \mathbf{c}_n \\ \mathbf{b}_n \end{Bmatrix} \tag{78}$$

The vectors $\mathbf{a}_n$ and $\mathbf{b}_n$ contains twelve components: three forces, three moments, three rotations and three displacements. Thus, the eigenvalue problem with respect to λ is, in effect, a problem of finding complex roots of a twelfth-order polynomial:

$$C_1\lambda^{12} + C_2\lambda^{11} + \cdots + C_{11}\lambda^2 + C_{12}\lambda + C_{13} = 0 \tag{79}$$

The parameter λ is expressed via propagation constant as

$$\lambda = \exp(iK_B) = \exp(-K_B^{\mathrm{Im}})\left(\cos(K_B^{\mathrm{Re}}) + i\sin(K_B^{\mathrm{Re}})\right) \tag{80}$$

The free wave propagation is impossible and filtering effect is achieved when all the 12 solutions fulfil the condition that $|\lambda| \neq 1$.

3.10. Power flow

Power flow in the structure performing time harmonic motion at the frequency ω is defined by following expression Miller and von Flotow [26], where "$*$" indicates the complex conjugate function:

$$\begin{aligned} \tilde{E}_{flux}(s) = {} & \tfrac{1}{2}\,\mathrm{Re}(R_u(s)(-i\omega)u(s)^*) + \tfrac{1}{2}\mathrm{Re}(R_v(s)(-i\omega)v(s)^*) \\ & + \tfrac{1}{2}\,\mathrm{Re}(R_w(s)(-\mathrm{i}\omega)w(s)^*) + \tfrac{1}{2}\mathrm{Re}(M_\alpha(s)(-\mathrm{i}\omega)\cdot\alpha(s)^*) \\ & + \tfrac{1}{2}\,\mathrm{Re}(M_\beta(s)(-i\omega)\beta(s)^*) + \tfrac{1}{2}\mathrm{Re}(M_\gamma(s)(-i\omega)\gamma(s)^*) \end{aligned} \tag{81}$$

It is a sum of six components which present contributions of longitudinal deformation, torsion and flexural deformation in two coordinate planes.

4. Standing and travelling waves in compound curved pipes

A number of examples of application of the described method of boundary integral equations are presented in this section. These examples are split into two categories: the eigenfrequency analysis of vibration of structures of the finite length and the power flow analysis in infinitely long structures.

4.1. Eigenfrequency analysis

In the case of free vibrations, the 'actual loading' case is represented as the absence of driving forces, $\mathbf{q}$=0 in Eq. (73), which then becomes

$$\mathbf{Bc} = 0 \tag{82}$$

Examples of calculations of eigenfrequencis are concerned with free in-plane and out-of-plan of planar vibrations of a single uniform segment of a curved pipe, see Fig. A.1. The eigenfrequencies of in-plane and out-of-plane motion are presented in the same non-dimensional form as used in Knag et al. [5] and Lee et al.[6], see Eq. (83) where the values for radius of gyration, ψ and Poisson ratio ν are listed. In these references, the used non-dimensional eigenfrequencies Ω' of the in-plane vibrations are reported, and the comparison is summarized in Table 3. Furthermore, commercial FE package

Table 3
Non-dimensional eigenfrequencies of the in-plane vibrations: boundary integral equation versus results reported in Knag et al. [5] and Lee et al. [6].

Mode	Boundary integral eq. (Love's gov. eq.)	Kang et al. (Love's gov. eq.)	Lee et al. (Flügge's gov. eq.)
In-plane non-dim. eigenfrq., Ω', for a segment with 5° angle of opening, clamped-clamped bc.			
1	1247.5675	1247.5675	1247.0700
2	2489.7481	2489.7481	2493.9590
3	2942.5805	–	2937.7038
4	3740.4334	3740.4334	3741.2092
In-plane non-dim. eigenfrq., Ω', for a segment with 5° angle of opening, free–free bc.			
1	1247.1131	1247.1131	1247.4466
2	2493.9771	2493.9771	2494.2896
3	2937.7679	2937.7679	2937.2384
4	3741.4749	3741.4749	3741.4112
In-plane non-dim. eigenfrq., Ω', for a segment with 180° angle of opening, clamped–clamped bc.			
1	4.3694551	4.3694551	4.3721593
2	9.4982704	9.4982704	9.5078102
3	17.7040140	17.704014	17.722215
4	25.6417085	25.641709	25.668470
In-plane non-dim. eigenfrq., Ω', for a segment with 180° angle of opening, free–free bc.			
1	1.8363460	1.8363460	1.8371547
2	5.3028579	5.3028579	5.3078041
3	11.0999717	11.099972	11.111971
4	18.9884643	18.988464	19.010617

Table 4
Non-dimensional eigenfrequencies of out-of-plane vibrations: boundary integral equation versus results obtained by use of ANSYS11 with beam44 elements.

Mode	Boundary integral eq.	ANSYS11 beam44	Boundary integral eq.	ANSYS11 beam44
	Out-of-plane non-dim. eigenfrq., Ω', for a segment with 5° angle of opening, free–free bc.		*Out-of-plane non-dim. eigenfrq., Ω', for a segment with 5° angle of opening, clamped–clamped bc.*	
1	774.0281	773.6	773.5448	773.5
2	1545.9006	1547.5	1546.7551	1546.7
3	2319.8549	2332.0	2319.6938	2320.6
4	2938.3143	2868.0	2938.4395	2917.2
	Out-of-plane non-dim. eigenfrq., Ω', for a segment with 180° angle of opening, free–free bc.		*Out-of-plane non-dim. eigenfrq., Ω', for a segment with 180° angle of opening, clamped–clamped bc.*	
1	4.119485	4.0993	1.817661	1.8167
2	9.105379	9.0329	5.237223	5.2270
3	16.935268	16.7430	10.987080	10.9420
4	21.293283	21.2010	18.834997	18.7010

ANSYS11 has been used for calculations of the non-dimensional eigenfrequencies of the out-of-plane free vibrations of the same structures, and comparison is summarized in Table 4:

$$\Omega' = \frac{\omega R^2}{\psi c_s} \quad \text{where} \quad \psi = \sqrt{\frac{J}{A_p}} = \sqrt{\frac{1}{1200}}, \quad R = 1 \ \text{and} \ \nu = 0.3 \tag{83}$$

The eigenfrequencies are calculated for uniform segments with 5° and 180° angles of opening for the two sets of boundary conditions: 'clamped–clamped' and 'free–free'.

The third example of the eigenfrequency analysis is more involved. It is concerned with calculations of eigenfrequencies of a spatial system where in-plane and out-of-plane motion cannot be separated. This structure has the shape of an 'elastic hook' made of an empty pipe with the outer diameter of 30 and 2 mm wall thickness, see Fig. 5. The results obtained by using boundary integral equations method are given in Table 5, together with the results obtained by the commercial FEM code, ANSYS11 using its beam44 elements, with the shear correction factor taken as k_s=0.56, see Eq. (84) [27]. Note that the largest discrepancy between the eigenfrequencies is 1.5 percent:

$$k_s = \frac{6(1+\nu)(1+m)^2}{(7+6\nu)(1+m)^2+(20+12\nu)m^2} \quad \text{where} \quad m = \frac{d_o - 2h}{d_o} \tag{84}$$

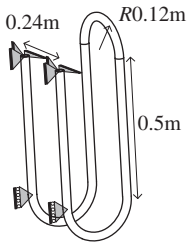

Fig. 5. The 'elastic hook'. Parameters of a curved pipe: diameter of 30 mm and a wall thickness of 2 mm, ρ_s=7800 kg/m^3, E=210 GPa and v=0.3.

Table 5
The first 20 eigenfrequencies found by the commercial FEM code ANSYS' with beam44 elements and by the boundary integral equations method, BIE, for the geometry at Fig. 5.

FEM (Hz)	8.492	26.04	26.23	30.90	55.72	103.4	107.7	163.0	190.2	240.3
BIE (Hz)	8.498	26.05	26.24	30.98	55.83	103.6	107.9	163.5	190.8	241.5
FEM (Hz)	272.0	336.9	343.5	407.6	424.9	449.1	531.4	627.9	764.5	784.9
BIE (Hz)	273.3	339.0	345.4	410.8	427.9	453.4	536.1	636.0	776.0	794.2

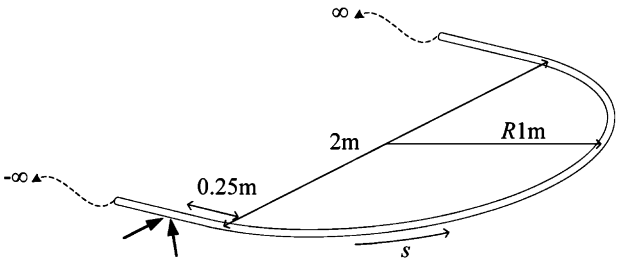

Fig. 6. The U-shaped pipe, pipe diameter 30 mm and wall thickness 2 mm, ρ_s=7800 kg/m^3, ρ_f=1000 kg/m^3, E=210 GPa and v=0.3. The wavy arrows designate infinitely long segments.

These examples demonstrate validity of the methodology employed in this paper and they serve as a verification of the codes, which implement this methodology. A simple modification of the codes is requested to address the power flow analysis in an infinite or semi-infinite piping system considered in Section 4.2.

4.2. Power flow analysis

In the case, when harmonic external forces are applied to the structure, Eq. (73) acquires the left hand side. For an infinite structure and for a finite structure with material losses taken into account, the determinant of this system of linear algebraic equations cannot vanish, and it has a unique solution, which defines the forced response: the whole set of state variables at the edges of each segment of a compound pipe. Then displacements, rotations, forces and moments in an arbitrary cross section of a pipe are readily available by employing the Somigliana's identities as described in Section 3.5. It facilitates the use of Eq. (60) to calculate the power flow through a set of selected cross sections in given excitation conditions.

In industrial and domestic piping systems, curved pipe segments are used in combination with the straight segments to control the global shape of a system. Typically, all segments of the piping system have the same outer diameter and wall thickness, so that the shape of a piping line is controlled by the curvature and the angle of opening of curved segments.

To illustrate the influence of discontinuities in the curvature of a pipe on its wave guide behaviour, the power flow in an U-shaped pipe, see Fig. 6, and in a S-shaped pipe system, see Fig. 7, are compared. Calculations are done in the frequency range from 1 to 1900 Hz. The results are given for a water filled pipe with an outer diameter of 30 mm and a wall thickness of 2 mm. The excitation by a vertical force and by the horizontal force is considered separately, both with amplitude of 10 N, see Figs. 6 and 7. The vertical force generates the out-of-plane motion which involves out-of-plane flexural deformation and torsion. The horizontal force produces the in-plane motion which involves in-plane flexural deformation and axial deformation.

The power flow in the structures sketched at Figs. 6 and 7 is presented in the 'insertion loss' (IL) format, where the power flow is a compound structure is scaled by the power flow in the reference structure. In this case, the

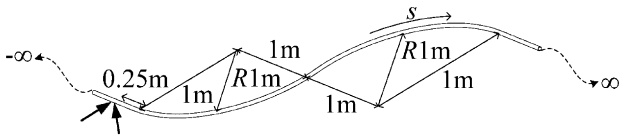

Fig. 7. The S-shaped pipe, pipe diameter 30 mm and wall thickness 2 mm, ρ_s=7800 kg/m^3, ρ_f=1000 kg/m^3, E=210 GPa and v=0.3. The wavy arrows designate infinitely long segments.

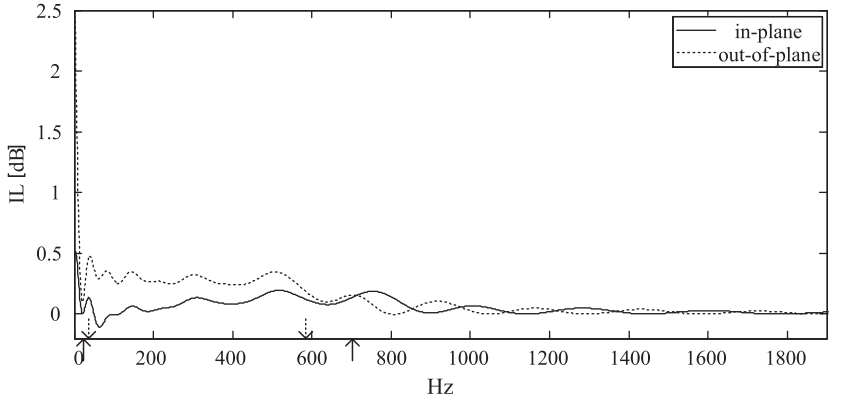

Fig. 8. The frequency-dependence of IL for the U-shaped pipe illustrated on Fig. 6: in-plane case solid line and out-of-plane dashed line.

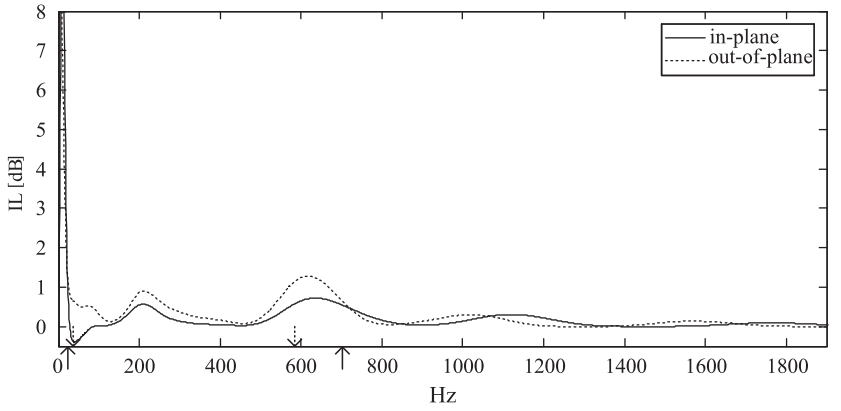

Fig. 9. The frequency-dependence of IL for the S-shaped pipe illustrated in Fig. 7: in-plane case solid line and out-of-plane dashed line.

reference is provided by the power flow in a straight uniform water-filled pipe of the same parameters. This quantity is introduced as

$$\mathrm{IL}\,[\mathrm{dB}] = 10\log\left(\frac{\tilde{E}_{\mathrm{ref}}}{\tilde{E}_{\mathrm{system}}}\right) \tag{85}$$

Here the reference power flow $\tilde{E}_{\mathrm{ref}}$ is readily available from a well known Green's function for flexural wave motion of a straight uniform pipe. Obviously, this reference is the same for the in-plane and out-of-plane excitation of U- and S-shaped pipe. The frequency-dependence of the IL for the U-shaped pipe is given in Fig. 8 and for the S-shaped pipe in Fig. 9.

The arrows in Figs. 8 and 9 designate the cut on and cut off frequencies, with the solid arrow for the in-plane case and the dashed arrow for the out-of-plane case. As a reference, the dispersion diagrams for curved segments are plotted in Fig. 10 (the 'in-plane' wavenumbers) and Fig. 11 (the 'out-of-plane' wavenumbers).

The differences between the U-shaped and the S-shaped models are most pronounced at low frequencies up to 25 Hz for the in-plane case and up to 35 Hz for the out-of-plane case. The S-shaped pipe has three discontinuities in the curvature, including the change of the sign, whereas the U-shaped pipe has two discontinuities. The fluctuations in

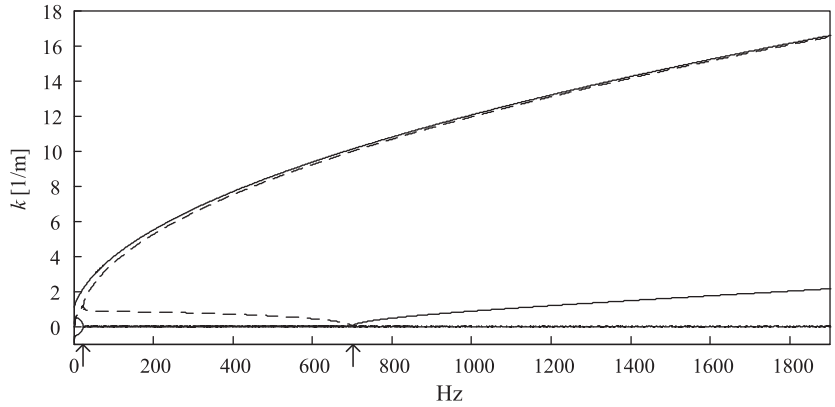

Fig. 10. Dimensional dispersion diagram (the in-plane case) for the curved pipe water filled segment used in the models shown in Figs. 6 and 7: real part solid line and imaginary part dashed line.

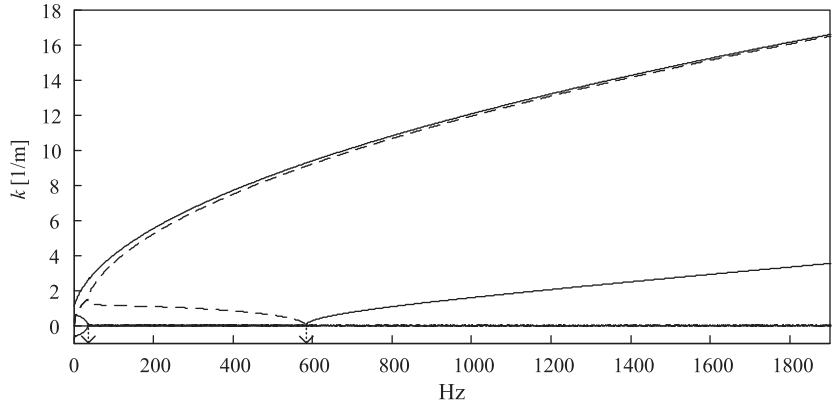

Fig. 11. Dimensional dispersion diagram (the out-of-plane case) for the curved pipe water filled segment used in the models shown in Figs. 6 and 7: real part solid line and imaginary part dashed line.

insertion loss are larger for the S-shaped pipe than for the U-shaped pipe. This indicates that the IL is more sensitive to the number of 'jumps' in curvature than to the length of curved segments.

At higher frequencies, this difference as well as the difference between the in-plane and the out-of-plane excitation diminishes. Furthermore, the magnitude or IL tends to zero, because the wavelengths become small in comparison with the radius of the segments. This tendency is seen most clearly when the excitation frequency get up in the domain where there both are travelling transversal and longitudinal/torsion waves, i.e. the frequencies right to both arrows.

5. Waves in periodic curved pipes

In this section, we consider three types of structures. In each case, however, a structure contains the same repeated spatial segments, which, in turn are composed of curved and straight pipe elements. To apply the Floquet theory and find propagation constants, the idealized model of an infinitely long structure is considered first. This modelling defines location of stop bands in the frequency domain. Next, we consider infinite structures composed of exactly the same segments as in the previous case, but the number of these repeated segments is fairly small. The 'outer' part of a piping system is then modelled as a simple straight pipe. The power flow analysis in the case of forced vibration is performed by means of the boundary integral equations method in the frequency range that covers pass bands and stop bands predicted by the Floquet theory. We are particularly concerned with the comparison of attenuation levels achieved with adding periodicity cell one by one. Finally, we consider forced vibrations of a structure of a finite length with no material losses by means of boundary integral equation method and by standard FE package ANSYS. At this stage, the point is to compare the shapes of standing waves, when the excitation frequency lies in the pass band or in the stop bands predicted by the Floquet theory for an unbounded structure.

5.1. Boundary integral equation method and Floquet theory—travelling wave analysis

A periodic structure consisting of curved and straight pipe segments shown in Fig. 12 is considered. The frequency dependence of the parameters $|\lambda|$ introduced as Eq. (79) is shown in Fig. 13. In accordance with the Floquet theory, the location of the frequency stop bands is defined by the condition $|\lambda| \neq 1$ held for all twelve roots of the characteristic equation (79). These predictions are compared with the power flow analysis, when a finite number of repeated substructures are inserted into an infinitely long structure.

The power flow in the structure shown in Fig. 14 versus excitation frequency is presented in Fig. 15 for variable number of the 'periodicity cells' inserted into a straight pipe. The stop band filter consists of two to eight chosen repeated substructures.

Here the concept of insertion losses is used again, see Eq. (85). The reference solution for the following examples is provided by the energy flux through a single periodic cell inserted in an otherwise uniform infinitely long water filled pipe. The power flow analysis is here performed for frequencies in between 1 and 955 Hz.

As it can be seen in the graphs in Fig. 15, the performance of the stop band filter is not much improved when the number of 'periodicity cells' becomes larger than five. On the other hand, it is notably to see that only two repeated substructures already gives a noticeable attenuation effect in several frequency stop bands. The stop bands predicted by the Floquet theory are marked as grey strips in Figs. 15 and 16. When looking at the graphs crossing the by grey bands marked stop-bands at Fig. 15, are the by Floquet theory idealized exponential decay rate per repeated 'periodic cell' clearly indicated, even for a relatively low number of repeated 'periodic cells'.

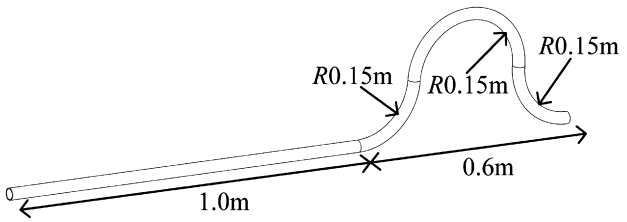

Fig. 12. The pipe segments used as the periodic repeated substructure; pipe diameter 30 mm and wall thickness 2 mm, ρ_s=7800 kg/m^3, ρ_f=1000 kg/m^3, E=210 GPa and v=0.3.

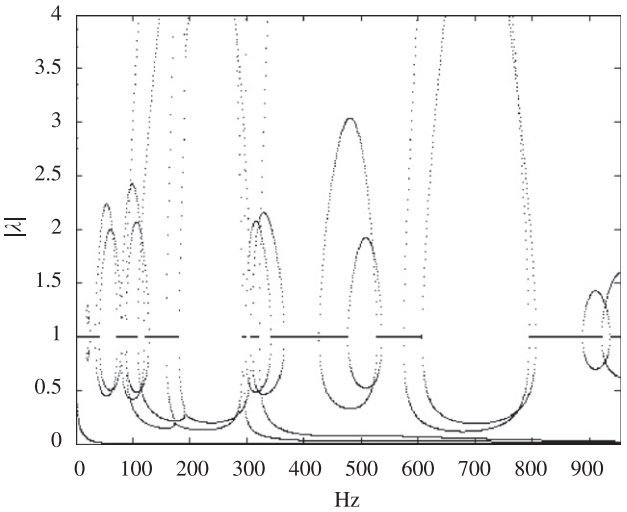

Fig. 13. The magnitude of $|\lambda|$ versus excitation frequency, stop bands are identified by condition $|\lambda| \neq 1$.

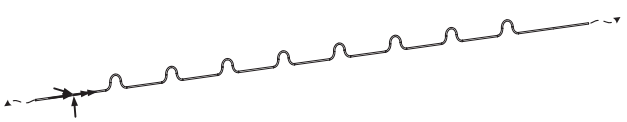

Fig. 14. An infinitely long pipe with the eight 'periodicity cells' inserted; pipe diameter 30 mm and wall thickness 2 mm, ρ_s=7800 kg/m^3, ρ_f=1000 kg/m^3, E=210 GPa and v=0.3. The wavy arrows designate infinitely long segments.

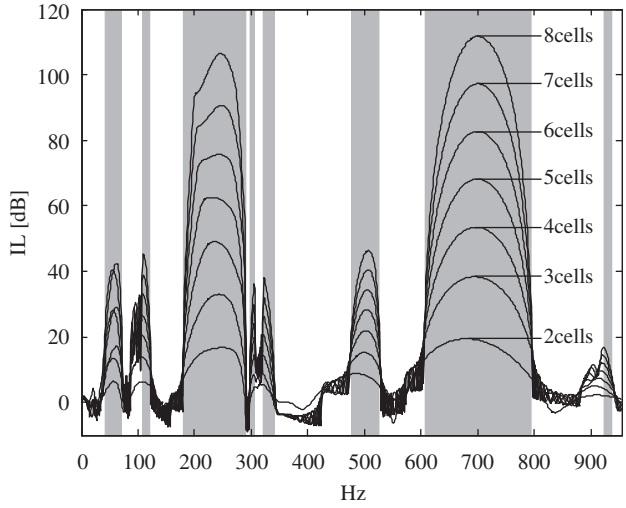

Fig. 15. Insertion losses in a pipe with variable number of inserted 'periodicity cells'. The grey strips indicate Floquet-predicted stop bands.

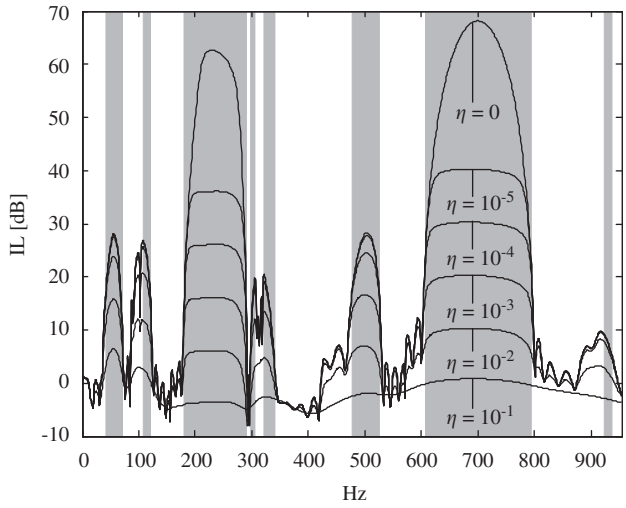

Fig. 16. Insertion losses in a pipe with five inserted 'periodicity cells' and variable material loss factor η. The grey strips indicate Floquet-predicted stop bands.

To illustrate the effect of structural damping on stop bands predicted by the Floquet theory, the power flow in several periodic pipes which have different magnitudes of the material losses is calculated. In these calculations, the standard model of materials losses as a complex Young's modulus defined by the loss factor, η given by Eq. (52) is employed. The analysis is performed for the pipe with five 'periodicity cells' shown in Fig. 12. Material losses are disregarded in the 'outer' infinitely long straight segments of the pipeline. As it can be seen in Fig. 16, for relatively small rates of structural damping, $\eta < 10^{-3}$, there is no significant change in the obtained stop-band behaviour. It can also be seen that when the damping ratio of η becomes large, the stop-band effect is masked by the overall damping.

The effect of repeated 'periodicity cells' in generation of frequency stop bands in an infinitely long structure is explained by the phenomenon of interference of waves reflected by these cells. In the case of forced response of a periodic infinite structure, this interference dramatically reduces its admittance. It results in the reduction of the energy input into the system and, therefore, in the suppression of travelling waves. However, the periodicity effect is also observed in the case of forced vibrations of a finite structure with no material losses.

5.2. *Floquet theory and FE method—standing wave analysis*

Forced vibrations of the structure shown in Fig. 17 are analysed by the Floquet theory and by the finite element code ANSYS11 using its beam44 elements where the shear stress factor is chosen to k_s=0.56, see Eq. (84) [27]. As already mentioned, the formulation of the Floquet theory involves the boundary integral equation method.

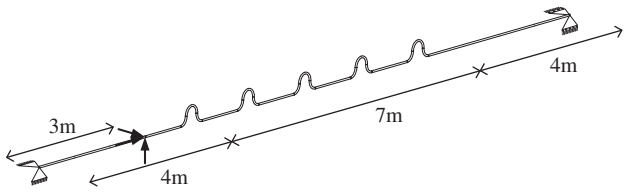

Fig. 17. The simple supported empty pipe with five periodicity cells inserted.

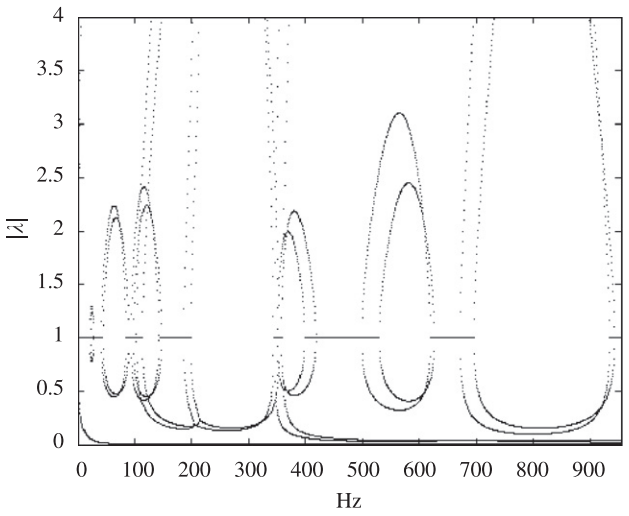

Fig. 18. The magnitude of $|\lambda|$ versus excitation frequency, stop-bands are identified by condition $|\lambda| \neq 1$.

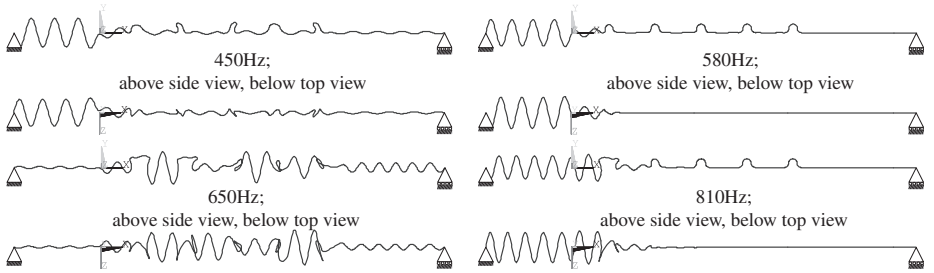

Fig. 19. Shapes of standing waves in the simple supported beam illustrated in Fig. 17, seen from side and top view, modelled by help of ANSYS11 with beam44 elements.

The simply supported beam is loaded by a point harmonic force at the distance 3 m from its left end. The force has the 10 N amplitude of components in each direction of the coordinate system. For the power flow in an infinitely long periodic structure, the Floquet theory predicts stop bands in the frequency ranges shown in Fig. 18. The shapes of forced vibrations (the shape of standing waves) for the excitation frequencies inside and outside stop bands obtained by the finite element method are shown in Fig. 19. As is seen, the excitation inside the stop bands generates the standing waves strongly localised between the left edge and the periodic inclusion. If the excitation frequency is not in the stop band, then the forced vibrations are such that the whole pipe is involved in the harmonic motion. The element length is here set to 0.02 m. These standing wave shapes are calculated for two excitation frequencies inside the predicted stop-bands 580 and 810 Hz and two outside 450 and 650 Hz, see Fig. 18.

5.3. Parametric study

As discussed in the previous sub-sections, insertion of several 'periodicity cells' shown in Fig. 12 in a straight pipe produces strong effect of suppression of wave propagation in an infinitely long structure and strong localisation effect in the shape of forced vibrations of a structure of finite length. This 'periodicity cell' has several geometry parameters, which

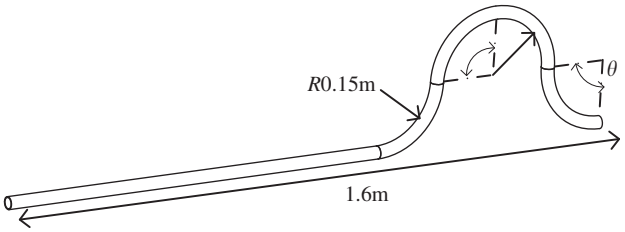

Fig. 20. The pipe segment employed as a periodicity cell. Radius of curvature is kept constant while angle of curvature θ are varied. Pipe diameter 30 mm and wall thickness 2 mm, ρ_s=7800 kg/m^3, E=210 GPa and v=0.3.

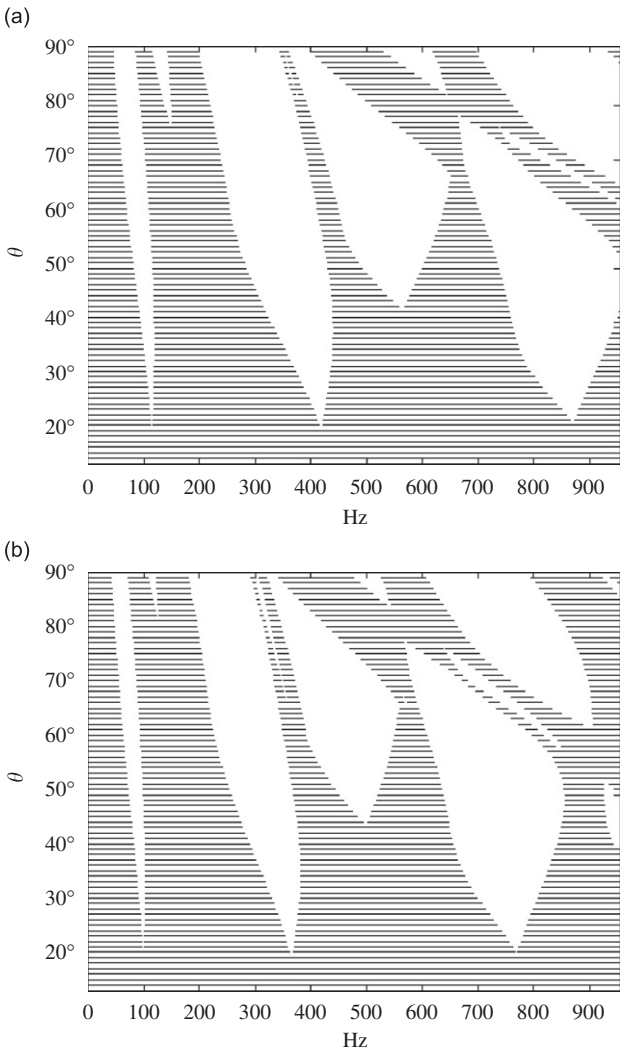

Fig. 21. Pass band $|\lambda|=1$ (shadowed) and stop bands $|\lambda|\neq 1$ (non-shadowed) for an infinitely long pipe: (a) an empty pipe and (b) a water-filled pipe, ρ_f=1000 kg/m^3.

may readily be tuned to produce the attenuation effect in prescribed frequency ranges. To illustrate possibility to tailor the location of the frequency stop bands, their boundaries, defined by the condition $|\lambda|=1$ are plotted in Figs. 20 and 21 for a pipe with and without water inside. In this figure, the pairs of the frequency and the angle of the opening of the segment, which fall into a stop band, are non-shadowed. In opposite, the combinations of these two parameters, which do not produce a stop band effect, are located in the shadowed zones.

As it is seen, tailoring of stop bands to the prescribed excitation frequencies is feasible by changing the geometry of the implemented sub-structure. Therefore, the stop-band effect can be used as a tool of passive control of vibrations in the piping system. It should be noted that the stop-band behaviour is not too sensitive to small changes in angle of curvature of the curved segments. The same holds true as regards the effect of fluid loading.

6. Conclusions

The findings reported in the paper are summarized as follows:

- location of dispersion curves for fluid-filled elastic pipes with parameters relevant to industrial and domestic piping system is weakly affected by the pressurization and by the velocity of the fluid. Therefore, the mass density appears to be the dominant fluid parameter for relatively stiff pipes filled with an inviscid fluid in the low frequency domain.
- the boundary integral equation method can be reliably used to model forced and free vibrations of compound arbitrary shaped structures with straight and curved pipe segments. Its predictions are shown to be in excellent agreement with the results of the eigenfrequency analysis by the commercial finite elements program ANSYS 11 and with previously published results for curved beams.
- insertion of a relatively small number of 'periodicity cells' in otherwise straight pipe produces a substantial attenuation of the power flow effect in the frequency ranges predicted by the classical Floquet theory for an infinitely periodic structure. The level of insertion losses tends to grow uniformly with the increase in the number of the periodicity cells. The material losses, when sufficiently large, mask the periodicity effect, rather than obscure it.
- the shape of standing wave in forced vibrations of a piping system of a finite length with several repeated 'periodicity cells' is strongly localised in the loaded span between the edge and periodic insertion when the excitation frequency falls into a stop band predicted by the classical Floquet theory. Otherwise, the amplitudes of forces vibrations have the same magnitudes along the whole pipe.
- it is feasible to tailor the filtering characteristics of a periodic insert in the frequency domain by varying parameters of geometry of a periodicity cell, such as the angle of opening of the curved segments and the length of segments. The level of attenuation is controlled by the number of periodicity cells and, therefore, can also be tuned to attain the required levels. This facilitates optimization of attenuation characteristics of the inserts, which lies beyond the scope of the present paper, but constitutes the subject of on-going research of the authors.

Acknowledgement

The financial support from the Danish agency for research and innovations is gratefully acknowledged.

Appendix A

The system of coordinates and the sign convention Figs. A.1–A.4.

Appendix B

The six unit point loading conditions

The considerations of the symmetry with respect to the loading point ξ yield the following loading conditions for two semi-infinitely segments in the six unit point load cases.

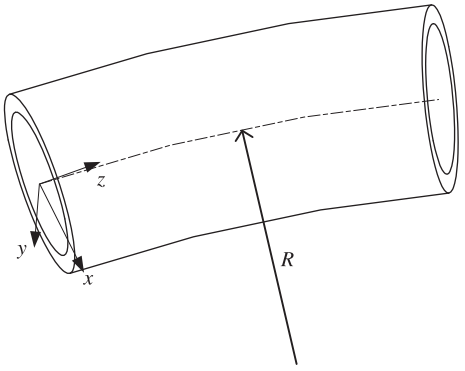

Fig. A1. The coordinate system.

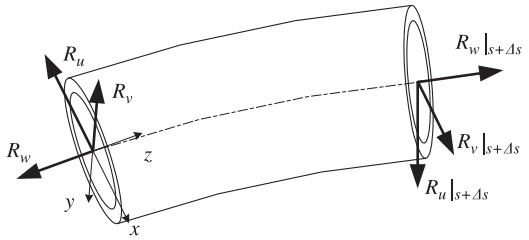

Fig. A2. The sign convention for forces.

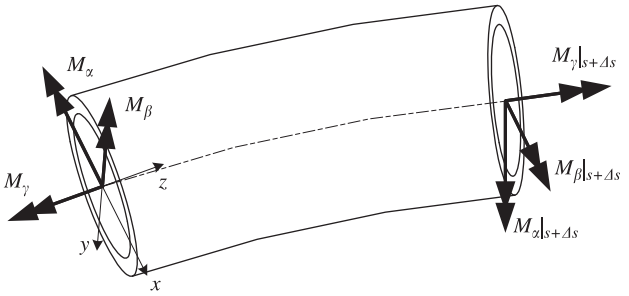

Fig. A3. The sign convention for moments.

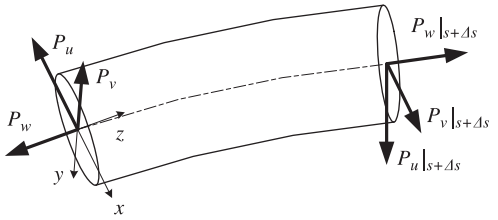

Fig. A4. The sign convention for pressure forces acting on a fluid segment.

For the three in-plane unit point load cases:

1. Unit point load case along x-axis at ξ:

$$Q_u(S)=\delta(S-\xi), Q_w(S)=0, Q_\beta(S)=0$$

$$\Downarrow$$

$$\hat{R}_u(S)=\frac{1+2B_A}{16}\left(-\frac{\partial^3 U}{\partial S^3}-\varepsilon\frac{\partial^2 W}{\partial S^2}\right)=-\frac{1}{2}\mathrm{sgn}(S-\xi),\quad \text{where}\quad S\to\xi$$

$$\Downarrow$$

$$\begin{cases} F_{11}^{ip}=\hat{R}_u(S)=-\dfrac{1}{2}\mathrm{sgn}(S-\xi) \\ G_{21}^{ip}=W(S)=0 \qquad\qquad \text{where}\quad S\to\xi \\ G_{31}^{ip}=\mathrm{B}(S)=0 \end{cases} \tag{B.1}$$

2. Unit point load case along z-axis at ξ:

$$Q_u(S)=0, Q_w(S)=\delta(S-\xi), \hat{q}_\beta(S)=0$$

$$\Downarrow$$

$$\hat{R}_w(S)=\frac{\partial W}{\partial S}-\varepsilon U=-\frac{1}{2}\mathrm{sgn}(S-\xi)\quad \text{where}\quad S\to\xi$$

$$\Downarrow$$

$$\begin{cases} G_{11}^{ip}=U(S)=0 \\ F_{21}^{ip}=\hat{R}_w(S)=-\dfrac{1}{2}\mathrm{sgn}(S-\xi)\quad \text{where}\quad S\to\xi \\ F_{31}^{ip}=\hat{M}_\beta(S)=0 \end{cases} \tag{B.2}$$

3. Unit point load case around y-axis at ξ:

$$\begin{gathered} Q_u(S)=0, Q_w(S)=0, Q_\beta(S)=\delta(S-\xi) \\ \Downarrow \\ \hat{M}_\beta(S)=\frac{1+2B_A}{16}\left(\frac{\partial^2 U}{\partial S^2}+\varepsilon\frac{\partial W}{\partial S}\right)=-\frac{1}{2}\mathrm{sgn}(S-\xi) \quad \text{where} \quad S\to\xi \\ \Downarrow \\ \begin{cases} G_{11}^{ip}=U(S)=0 \\ F_{21}^{ip}=\hat{R}_w(S)=0 \qquad\qquad \text{where} \quad S\to\xi \\ F_{31}^{ip}=\hat{M}_\beta(S)=-\dfrac{1}{2}\mathrm{sgn}(S-\xi) \end{cases} \end{gathered} \tag{B.3}$$

For the three in-plane unit point load cases:

1. Unit point load case along y-axis at ξ:

$$\begin{gathered} Q_v(S)=\delta(S-\xi), Q_\gamma(S)=0, Q_\alpha(S)=0 \\ \Downarrow \\ \begin{cases} \hat{R}_v(S)=\dfrac{1+2B_A}{16}\left(-\dfrac{\partial^3 V}{\partial S^3}+\varepsilon\dfrac{\partial \Gamma}{\partial S}\right)+\dfrac{1+2B_A}{16(1+\nu)}\left(\varepsilon\dfrac{\partial \Gamma}{\partial S}+\varepsilon^2\dfrac{\partial V}{\partial S}\right)=-\dfrac{1}{2}\mathrm{sgn}(S-\xi), \\ \qquad\qquad \text{where} \quad S\to\xi \end{cases} \\ \Downarrow \\ \begin{cases} F_{11}^{op}=\hat{R}_v(S)=-\dfrac{1}{2}\mathrm{sgn}(S-\xi) \\ F_{21}^{op}=\hat{M}_\gamma(S)=0 \qquad\qquad \text{where} \quad S\to\xi \\ G_{31}^{op}=\mathrm{A}(S)=0 \end{cases} \end{gathered} \tag{B.4}$$

2. Unit point load case around z-axis at ξ:

$$\begin{gathered} Q_v(S)=0,\ Q_\gamma(S)=\delta(S-\xi), Q_\alpha(S)=0 \\ \Downarrow \\ \hat{M}_\gamma(S)=\frac{1+2B_A}{16(1+\nu)}\left(\frac{\partial \Gamma}{\partial S}+\varepsilon\frac{\partial V}{\partial S}\right)=-\frac{1}{2}\mathrm{sgn}(S-\xi) \quad \text{where} \quad S\to\xi \\ \Downarrow \\ \begin{cases} F_{11}^{op}=\hat{R}_v(S)=0 \\ F_{21}^{op}=\hat{M}_\gamma(S)=-\dfrac{1}{2}\mathrm{sgn}(S-\xi) \quad \text{where} \quad S\to\xi \\ G_{31}^{op}=\mathrm{A}(S)=0 \end{cases} \end{gathered} \tag{B.5}$$

3. Unit point load case around x-axis at ξ:

$$\begin{gathered} Q_v(S)=0, Q_\gamma(S)=0, Q_\alpha(S)=\delta(S-\xi) \\ \Downarrow \\ \hat{M}_\gamma(S)=\frac{1+2B_A}{16}\left(-\frac{\partial^2 V}{\partial S^2}+\varepsilon\Gamma\right)=-\frac{1}{2}\mathrm{sgn}(S-\xi) \quad \text{where} \quad S\to\xi \\ \Downarrow \\ \begin{cases} G_{11}^{op}=V(S)=0 \\ G_{21}^{op}=\Gamma(S)=0 \qquad\qquad \text{where} \quad S\to\xi \\ F_{31}^{op}=\hat{M}_\gamma(S)=-\dfrac{1}{2}\mathrm{sgn}(S-\xi) \end{cases} \end{gathered} \tag{B.6}$$

Appendix C

Expressions for $\mathbf{H}^{ip}$, $\mathbf{H}^{op}$, $\boldsymbol{\chi}^{ip}$, $\boldsymbol{\chi}^{op}$, $\boldsymbol{\varphi}^{ip}$ and $\boldsymbol{\varphi}^{op}$ in Green's matrix

The components in matrix $\mathbf{H}^{ip}$ for the In-plane case:

$$H_{11}^{ip}=\frac{8i}{(1+2B_A)}\frac{m_3^wK_2^{ip}-m_2^wK_3^{ip}}{\left(m_3^wK_1^{ip}+\varepsilon m_1^wm_3^w\right)K_1^{ip^2}K_2^{ip}-\left(m_2^wK_1^{ip}+\varepsilon m_1^wm_2^w\right)K_1^{ip^2}K_3^{ip}+\left(m_1^wK_2^{ip}+\varepsilon m_1^wm_2^w\right)K_2^{ip^2}K_3^{ip}-\left(m_3^wK_2^{ip}+\varepsilon m_2^wm_3^w\right)K_2^{ip^2}K_1^{ip}+\left(m_2^wK_3^{ip}+\varepsilon m_2^wm_3^w\right)K_3^{ip^2}K_1^{ip}-\left(m_1^wK_3^{ip}+\varepsilon m_1^wm_3^w\right)K_3^{ip^2}K_2^{ip}} \tag{C.1}$$

$$H_{12}^{ip}=\frac{8i}{(1+2B_A)}\frac{m_1^wK_3^{ip}-m_3^wK_1^{ip}}{\left(m_3^wK_1^{ip}+\varepsilon m_1^wm_3^w\right)K_1^{ip^2}K_2^{ip}-\left(m_2^wK_1^{ip}+\varepsilon m_1^wm_2^w\right)K_1^{ip^2}K_3^{ip}+\left(m_1^wK_2^{ip}+\varepsilon m_1^wm_2^w\right)K_2^{ip^2}K_3^{ip}-\left(m_3^wK_2^{ip}+\varepsilon m_2^wm_3^w\right)K_2^{ip^2}K_1^{ip}+\left(m_2^wK_3^{ip}+\varepsilon m_2^wm_3^w\right)K_3^{ip^2}K_1^{ip}-\left(m_1^wK_3^{ip}+\varepsilon m_1^wm_3^w\right)K_3^{ip^2}K_2^{ip}} \tag{C.2}$$

$$H_{13}^{ip}=\frac{8i}{(1+2B_A)}\frac{m_2^wK_1^{ip}-m_1^wK_2^{ip}}{\left(m_3^wK_1^{ip}+\varepsilon m_1^wm_3^w\right)K_1^{ip^2}K_2^{ip}-\left(m_2^wK_1^{ip}+\varepsilon m_1^wm_2^w\right)K_1^{ip^2}K_3^{ip}+\left(m_1^wK_2^{ip}+\varepsilon m_1^wm_2^w\right)K_2^{ip^2}K_3^{ip}-\left(m_3^wK_2^{ip}+\varepsilon m_2^wm_3^w\right)K_2^{ip^2}K_1^{ip}+\left(m_2^wK_3^{ip}+\varepsilon m_2^wm_3^w\right)K_3^{ip^2}K_1^{ip}-\left(m_1^wK_3^{ip}+\varepsilon m_1^wm_3^w\right)K_3^{ip^2}K_2^{ip}} \tag{C.3}$$

$$H_{21}^{ip}=\frac{1}{2}\frac{K_3^{ip^2}+\varepsilon m_3^wK_3^{ip}-K_2^{ip^2}-\varepsilon m_2^wK_2^{ip}}{m_1^wK_1^{ip}(K_3^{ip2}-K_2^{ip^2})+m_2^wK_2^{ip}(K_1^{ip^2}-K_3^{ip^2})+m_3^wK_3^{ip}(K_2^{ip^2}-K_1^{ip^2})} \tag{C.4}$$

$$H_{22}^{ip}=\frac{1}{2}\frac{K_1^{ip^2}+\varepsilon m_1^wK_1^{ip}-K_3^{ip^2}-\varepsilon m_3^wK_3^{ip}}{m_1^wK_1^{ip}(K_3^{ip^2}-K_2^{ip^2})+m_2^wK_2^{ip}(K_1^{ip^2}-K_3^{ip^2})+m_3^wK_3^{ip}(K_2^{ip^2}-K_1^{ip^2})} \tag{C.5}$$

$$H_{23}^{ip}=\frac{1}{2}\frac{K_2^{ip^2}+\varepsilon m_2^wK_2^{ip}-K_1^{ip^2}-\varepsilon m_1^wK_1^{ip}}{m_1^wK_1^{ip}(K_3^{ip^2}-K_2^{ip^2})+m_2^wK_2^{ip}(K_1^{ip^2}-K_3^{ip^2})+m_3^wK_3^{ip}(K_2^{ip^2}-K_1^{ip^2})} \tag{C.6}$$

$$H_{31}^{ip}=\frac{8}{(1+2B_A)}\frac{m_2^wK_2^{ip}-m_3^wK_3^{ip}}{m_1^wK_1^{ip}(K_3^{ip^2}-K_2^{ip^2})+m_2^wK_2^{ip}(K_1^{ip^2}-K_3^{ip^2})+m_3^wK_3^{ip}(K_2^{ip^2}-K_1^{ip^2})} \tag{C.7}$$

$$H_{32}^{ip}=\frac{8}{(1+2B_A)}\frac{m_3^wK_3^{ip}-m_1^wK_1^{ip}}{m_1^wK_1^{ip}(K_3^{ip^2}-K_2^{ip^2})+m_2^wK_2^{ip}(K_1^{ip^2}-K_3^{ip^2})+m_3^wK_3^{ip}(K_2^{ip^2}-K_1^{ip^2})} \tag{C.8}$$

$$H_{33}^{ip}=\frac{8}{(1+2B_A)}\frac{m_1^wK_1^{ip}-m_2^wK_2^{ip}}{m_1^wK_1^{ip}(K_3^{ip^2}-K_2^{ip^2})+m_2^wK_2^{ip}(K_1^{ip^2}-K_3^{ip^2})+m_3^wK_3^{ip}(K_2^{ip^2}-K_1^{ip^2})} \tag{C.9}$$

The components in matrix $\mathbf{H}^{op}$ for the out-of-plane case:

$$H_{11}^{op}=\frac{8i}{(1+2B_A)}\frac{m_3^\gamma-m_2^\gamma}{K_1^{op}(m_1^\gamma(K_2^{op^2}-K_3^{op^2})+m_2^\gamma(K_3^{op^2}-K_1^{op^2})+m_3^\gamma(K_1^{op^2}-K_2^{op^2}))} \tag{C.10}$$

$$H_{12}^{op}=\frac{8i}{(1+2B_A)}\frac{m_1^\gamma-m_3^\gamma}{K_2^{op}(m_1^\gamma(K_2^{op^2}-K_3^{op^2})+m_2^\gamma(K_3^{op^2}-K_1^{op^2})+m_3^\gamma(K_1^{op^2}-K_2^{op^2}))} \tag{C.11}$$

$$H_{13}^{op}=\frac{8i}{(1+2B_A)}\frac{m_2^\gamma-m_1^\gamma}{K_3^{op}(m_1^\gamma(K_2^{op^2}-K_3^{op^2})+m_2^\gamma(K_3^{op^2}-K_1^{op^2})+m_3^\gamma(K_1^{op^2}-K_2^{op^2}))} \tag{C.12}$$

$$H_{21}^{op}=\frac{8i}{(1+2B_A)}\frac{(1+\nu)\left(iK_3^{op^2}-\varepsilon m_3^\gamma-iK_2^{op^2}+\varepsilon m_2^\gamma\right)+\varepsilon\left(m_2^\gamma-m_3^\gamma\right)}{K_1^{op}(m_1^\gamma(K_2^{op^2}-K_3^{op^2})+m_2^\gamma(K_3^{op^2}-K_1^{op^2})+m_3^\gamma(K_1^{op^2}-K_2^{op^2}))} \tag{C.13}$$

$$H_{22}^{op}=\frac{8i}{(1+2B_A)}\frac{(1+\nu)\left(iK_1^{op^2}-\varepsilon m_1^{\gamma}-iK_3^{op^2}+\varepsilon m_3^{\gamma}\right)+\varepsilon\left(m_3^{\gamma}-m_1^{\gamma}\right)}{K_2^{op}(m_1^{\gamma}(K_2^{op^2}-K_3^{op^2})+m_2^{\gamma}(K_3^{op^2}-K_1^{op^2})+m_3^{\gamma}(K_1^{op^2}-K_2^{op^2}))} \tag{C.14}$$

$$H_{23}^{op}=\frac{8i}{(1+2B_A)}\frac{(1+\nu)\left(iK_2^{op^2}-\varepsilon m_2^{\gamma}-iK_1^{op^2}+\varepsilon m_1^{\gamma}\right)+\varepsilon\left(m_1^{\gamma}-m_2^{\gamma}\right)}{K_3^{op}(m_1^{\gamma}(K_2^{op^2}-K_3^{op^2})+m_2^{\gamma}(K_3^{op^2}-K_1^{op^2})+m_3^{\gamma}(K_1^{op^2}-K_2^{op^2}))} \tag{C.15}$$

$$H_{31}^{op}=\frac{8}{(1+2B_A)}\frac{m_2^{\gamma}-m_3^{\gamma}}{m_1^{\gamma}(K_2^{op^2}-K_3^{op^2})+m_2^{\gamma}(K_3^{op^2}-K_1^{op^2})+m_3^{\gamma}(K_1^{op^2}-K_2^{op^2})} \tag{C.16}$$

$$H_{32}^{op}=\frac{8}{(1+2B_A)}\frac{m_3^{\gamma}-m_1^{\gamma}}{m_1^{\gamma}(K_2^{op^2}-K_3^{op^2})+m_2^{\gamma}(K_3^{op^2}-K_1^{op^2})+m_3^{\gamma}(K_1^{op^2}-K_2^{op^2})} \tag{C.17}$$

$$H_{33}^{op}=\frac{8}{(1+2B_A)}\frac{m_1^{\gamma}-m_2^{\gamma}}{m_1^{\gamma}(K_2^{op^2}-K_3^{op^2})+m_2^{\gamma}(K_3^{op^2}-K_1^{op^2})+m_3^{\gamma}(K_1^{op^2}-K_2^{op^2}))} \tag{C.18}$$

Matrix $\boldsymbol{\chi}^{ip}$ for the in-plane case:

$$\boldsymbol{\chi}^{ip}=\begin{bmatrix}1 & \mathrm{sgn}(S-\xi) & \mathrm{sgn}(S-\xi)\\ \mathrm{sgn}(S-\xi) & 1 & 1\\ \mathrm{sgn}(S-\xi) & 1 & 1\end{bmatrix} \tag{C.19}$$

Matrix $\boldsymbol{\chi}^{op}$ for the out-of-plane case:

$$\boldsymbol{\chi}^{op}=\begin{bmatrix}1 & 1 & \mathrm{sgn}(S-\xi)\\ 1 & 1 & \mathrm{sgn}(S-\xi)\\ \mathrm{sgn}(S-\xi) & \mathrm{sgn}(S-\xi) & 1\end{bmatrix} \tag{C.20}$$

Matrix $\boldsymbol{\varphi}^{ip}$ for the in-plane case:

$$\boldsymbol{\varphi}^{ip}=\begin{bmatrix}\mathrm{sgn}(S-\xi) & 1 & 1\\ 1 & \mathrm{sgn}(S-\xi) & \mathrm{sgn}(S-\xi)\\ 1 & \mathrm{sgn}(S-\xi) & \mathrm{sgn}(S-\xi)\end{bmatrix} \tag{C.21}$$

Matrix $\boldsymbol{\varphi}^{op}$ for the out-of-plane case:

$$\boldsymbol{\varphi}^{op}=\begin{bmatrix}\mathrm{sgn}(S-\xi) & \mathrm{sgn}(S-\xi) & 1\\ \mathrm{sgn}(S-\xi) & \mathrm{sgn}(S-\xi) & 1\\ 1 & 1 & \mathrm{sgn}(S-\xi)\end{bmatrix} \tag{C.22}$$

References

[1] M.P. Païdoussis., *Fluid–structure interactions slender structures and axial flow, vol. 1*, Academic Press, California, 1998.
[2] A.K. Misra, M.P. Païdoussis, K.S. Van, On the dynamics of curved pipes transporting fluid. Part I: Inextensible theory, *Journal of Fluid and Structures* 2 (1988) 221–244.
[3] A.K. Misra, M.P. Païdoussis, K.S. Van, On the dynamics of curved pipes transporting fluid. Part II: Extensible theory, *Journal of Fluid and Structures* 2 (1988) 245–261.
[4] S.J. Walsh, R.G. White, Vibrational power transmission in curved beams, *Journal of Sound and Vibration* 233 (2000) 455–488.
[5] B. Kang, C.H. Riedel, C.A. Tan, Free vibration analysis of planar curved beams by wave propagation, *Journal of Sound and Vibration* 260 (2003) 19–44.
[6] S.-K. Lee, B.R. Mace, M.J. Brennan, Wave propagation, reflection and transmission in curved beams, *Journal of Sound and Vibration* 306 (2007) 636–656.
[7] S.V. Sorokin, N. Olhoff, O.A. Ershova, Analysis of energy transmission in spatial piping systems with heavy internal fluid loading, *Journal of Sound and Vibration* 310 (2008) 1141–1166.
[8] J.F. Doyle., *Wave Propagation in Structures*, Springer, New York, 1997.
[9] J.R. Banerjee, Dynamical stiffness formulation for structural elements: a general approach, *Computers & structures* 63 (1997) 101–103.
[10] U. Lee, J. Kim, A.Y.T. Leung., The spectral element method in structural dynamics, *The Shock and Vibration Digest* 32 (2000) 451–465.
[11] U. Lee., *Spectral Element Method in Structural Dynamics*, John Wiley & Sons (Asia), Singapore, 2009.
[12] R. Davis, R.D. Henshell, G.B. Warburton, Constant curvature beam finite elements for in-plane vibrations, *Journal of Sound and Vibration* 25 (1972) 561–576.
[13] L. Brillouin., *Wave Propagation in Periodic Structures*, *second edition*, Dover Publications, New York, 1953.
[14] D.J. Mead., *Passive Vibration Control*, John Wiley & Sons, England, 1998.
[15] D.J. Mead, Wave propagation in continuous periodic structures: research contributions from Southampton, 1964–1995, *Journal of Sound and Vibration* 190 (1996) 495–524.
[16] S.V. Sorokin, O.A. Ershova, Plane wave propagation and frequency band gaps in periodic plates and cylindrical shells with and without heavy fluid loading, *Journal of Sound and Vibration* 278 (2004) 501–526.
[17] S.V. Sorokin, O.A. Ershova, Analysis of the energy transmission in compound cylindrical shells with and without internal heavy fluid loading by boundary integral equations and by Floquet theory, *Journal of Sound and Vibration* 291 (2006) 81–99.
[18] A.E.H. Love., *A treatise on the mathematical theory of elasticity*, *fourth edition*, Dover Publications, New York, 1927 reprint 1944.
[19] W.H. Wittrick, On elastic wave propagation in helical springs, *International Journal of Mechanical Science* 8 (1966) 25–47.

[20] S.V. Sorokin, Linear dynamics of elastic helical springs: asymptotic analysis of wave propagation, *Proceedings of Royal Society of London. — Mathematical, Physical, and Engineering Sciences* 465 (2009) 1513–1537.
[21] A.V. Sveshnikov, The limit absorption principle for a wave guide, *Doklady Akademii Nauk SSSR* 80 (1951) 345–347.
[22] B.R. Vainberg, *Asymtotic Methods in Equations of Mathematical Physics*, Gordon & Breach, 1988.
[23] S.S. Rau., *Mechanical vibrations*, *fourth edition*, Pearson Prentice Hall, New Jersey, 2004.
[24] W. Wunderlich, W.D. Pilkey., in: *Mechanics of Structures Variational and Computational Methods*, *second edition*, CRC Press, Florida, 2003.
[25] M.G. Floquet, Sur les equations differentielles linéaires á coefficents périodiques (in French), *Annales Scientifiques de L'É.N.S.* 2 (1883) 47–88.
[26] D.W. Miller, A. von Flotow, A travelling wave approach to power flow in structural networks, *Journal of Sound and Vibration* 128 (1989) 145–162.
[27] I.H. Shames, C.L. Dym., *Energy and Finite Element Methods in Structural Mechanics*, Tayler & Francis, New York, 1991.